iScience

Article

Distinct microRNA signatures define sporadic PSP-RS and PD in patient-derived midbrain organoids

Graphical abstract

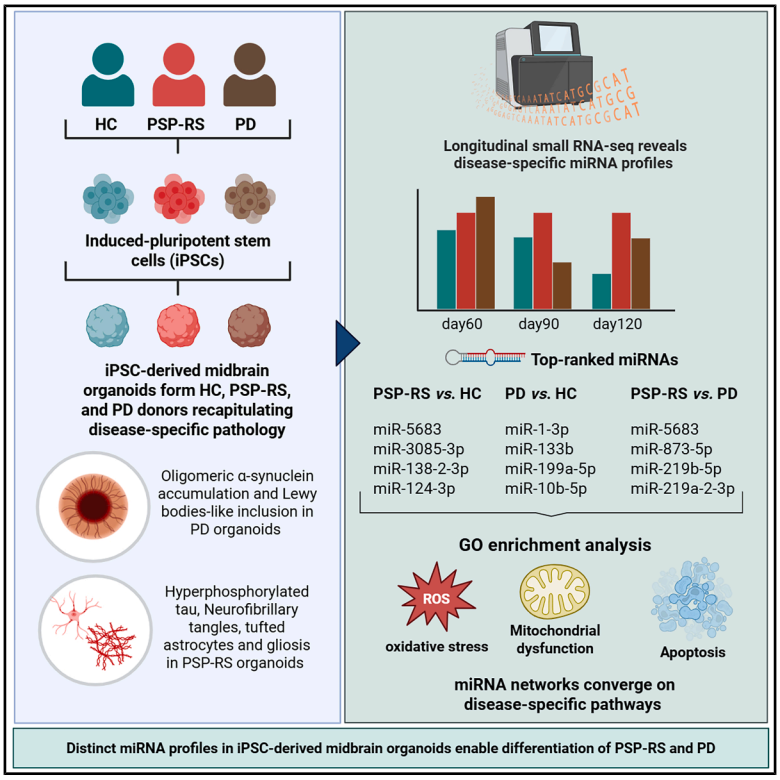

Highlights

- iPSC midbrain organoids model PSP-RS and PD with disease-specific features
- Distinct miRNA signatures differentiate PSP-RS, PD, and healthy controls
- miR-5683, miR-873-5p, and miR-219 family differentiate PSP-RS from PD

Authors

Desirèe Valente, Clara Zannino, Stefania Scalise, ..., Aldo Quattrone, Elvira Immacolata Parrotta, Giovanni Cuda

Correspondence

parrotta@unicz.it

In brief

Natural sciences; Biological sciences; Neuroscience; Cellular neuroscience

Valente et al., 2025, iScience *28*, 113162
August 15, 2025 © 2025 The Author(s). Published by Elsevier Inc.
https://doi.org/10.1016/j.isci.2025.113162

CellPress

iScience

CellPress
OPEN ACCESS

Article

Distinct microRNA signatures define sporadic PSP-RS and PD in patient-derived midbrain organoids

Desirèe Valente,[1,7] Clara Zannino,[1,7] Stefania Scalise,[1,7] Davide Bressan,[2] Valeria Lucchino,[1] Ermes Filomena,[3] Giorgia Lucia Benedetto,[4] Ida Lazzinnaro,[4] Mariagrazia Talarico,[4] Andrea Quattrone,[4] Fulvio Chiacchiera,[2] Graziano Pesole,[3,5] Aldo Quattrone,[6] Elvira Immacolata Parrotta,[4,9,*] and Giovanni Cuda[1,8]

[1]Department of Experimental and Clinical Medicine, University "Magna Graecia" of Catanzaro, 88100 Catanzaro, Italy
[2]Department of Cellular, Computational and Integrative Biology (CIBIO), University of Trento, 38123 Trento, Italy
[3]Department of Biosciences, Biotechnology and Environment, University of Bari Aldo Moro, 70125 Bari, Italy
[4]Department of Medical and Surgical Sciences, University "Magna Graecia" of Catanzaro, 88100 Catanzaro, Italy
[5]Institute of Biomembranes, Bioenergetics and Molecular Biotechnologies, National Research Council, 70126 Bari, Italy
[6]Institute of Neurology, University "Magna Graecia" of Catanzaro, 88100 Catanzaro, Italy
[7]These authors contributed equally
[8]Senior author
[9]Lead contact
*Correspondence: parrotta@unicz.it
https://doi.org/10.1016/j.isci.2025.113162

SUMMARY

Progressive supranuclear Palsy–Richardson syndrome (PSP-RS) is a rare, rapidly progressive tauopathy often misdiagnosed as Parkinson's disease (PD) due to overlapping clinical features and the lack of reliable molecular biomarkers. To address this need, we generated human midbrain organoids from induced pluripotent stem cells (iPSCs) derived from individuals with sporadic PSP-RS, PD, and healthy controls (HCs), and performed longitudinal small RNA sequencing to profile microRNA (miRNA) signatures. These 3D organoids recapitulated disease-relevant pathologies, including tau hyperphosphorylation in PSP-RS and α-synuclein aggregation in PD. Transcriptomic analysis revealed dynamic, disease-specific miRNA signatures. Notably, miR-5683, miR-873-5p, miR-219b-5p, and miR-219a-2-3p were enriched in PSP-RS, while PD organoids showed increased expression of miR-1-3p and miR-133b. Differential expression analysis identified miR-5683, miR-3085-3p, and miR-124-3p as robust classifiers distinguishing PSP-RS from controls. Our findings support iPSC-derived midbrain organoids as a relevant platform for modeling atypical parkinsonian syndromes and uncovering candidate miRNA biomarkers for early and differential diagnosis.

INTRODUCTION

Neurodegenerative disorders such as Parkinson's disease (PD) and progressive supranuclear Palsy–Richardson syndrome (PSP-RS) impose a growing burden on aging populations worldwide. Although these diseases have distinct molecular etiologies—α-synuclein aggregation in PD and tau hyperphosphorylation and aggregation in PSP-RS—patients often exhibit overlapping early motor symptoms, leading to frequent misdiagnosis and delays in appropriate clinical management.[1,2] There is a critical unmet need for robust biomarkers capable of distinguishing these conditions at early, clinically ambiguous stages. PD is primarily characterized by the progressive degeneration of dopaminergic neurons in the substantia nigra and the pathological accumulation of α-synuclein, manifesting in bradykinesia, rigidity, and resting tremor.[3,4] In contrast, PSP-RS, the most prevalent clinical phenotype within the spectrum of progressive supranuclear palsy disorders, is marked by the widespread deposition of hyperphosphorylated tau in the midbrain, basal ganglia, and brainstem.[5] However, early-stage symptoms overlap between PD and PSP-RS and often mask these distinct molecular signatures,[1,6] complicating timely and accurate diagnosis. MicroRNAs (miRNAs), a class of small non-coding RNAs that modulate gene expression post-transcriptionally, have emerged as promising candidates for understanding the molecular underpinnings of neurodegenerative diseases. In the central nervous system (CNS), miRNAs play pivotal roles in cellular processes relevant to disease pathogenesis, including mitochondrial dysfunction, autophagy, protein aggregation, apoptosis, and neuroinflammation.[7–12] Their remarkable stability in biofluids and disease-specific expression patterns support their utility as both mechanistic effectors and potential biomarkers.[13–15] Nevertheless, direct sampling of CNS tissue is rarely feasible in living patients, and while peripheral sources such as blood and cerebrospinal fluid (CSF) offer more accessible options, they may not accurately reflect brain-specific miRNA dynamics, particularly in

This is an open access article under the CC BY-NC license (http://creativecommons.org/licenses/by-nc/4.0/).

early disease stages.[16] Previous studies have identified altered miRNA levels in blood from PD patients (e.g., miR-1-3p, miR-22-5p, and miR-29a-3p),[17] and in plasma from individuals with multiple system atrophy (MSA) (e.g., miR-24, miR-148b, miR-223, miR-324-3p, miR-339-5p).[18] However, these findings often lack disease-contextual modeling and require further validation in more representative systems. To address these limitations, we employed induced pluripotent stem cell (iPSC)-derived midbrain organoids as a human-relevant *in vitro* model to investigate miRNA dysregulation in PSP-RS and PD. These 3D organoids replicate key features of midbrain architecture, including the presence of dopaminergic neurons, glial cell populations, and hallmark disease-related proteinopathies.[19,20] Next, we performed small RNA sequencing on midbrain organoids generated from patients with sporadic PSP-RS, PD, and neurologically healthy controls (HCs) across multiple developmental time points to uncover miRNA signatures with diagnostic potential. Our findings reveal distinct and temporally consistent miRNA expression profiles that differentiate PSP-RS from both PD and healthy controls, as well as PD from controls, establishing a framework for the future development of miRNA-based biomarkers for early and accurate differential diagnosis of parkinsonian syndromes.

RESULTS

Midbrain organoids recapitulate key molecular and cellular features of the human midbrain

To model PD and PSP-RS in a physiologically relevant system, we generated iPSCs from four patients with sporadic PD, four with sporadic PSP-RS, and three healthy controls (HCs). A comprehensive list of single nucleotide variants (SNVs) associated with late-onset PD and PSP-RS is provided in Table S1. These variants were analyzed in our patient cohort using whole-genome sequencing data from our donor-derived lines. For PD, we specifically analyzed *SNCA*, *LRRK2*, *VPS35*, and *GBA*; for PSP, we analyzed *MAPT*. No causative or likely pathogenic variants were identified in any of the samples, supporting the notion that our patients are indeed sporadic. Demographic and clinical data for PSP-RS patients and healthy donors, previously reported,[21] are summarized in Table S2, together with corresponding information for PD patients. iPSCs from each group were pooled to generate representative midbrain organoids that capture disease-specific molecular phenotypes. This approach was adapted to minimize batch-specific technical variability and to enhance the detection of convergent, disease-associated miRNA signatures across multiple sporadic donors with PSP-RS and PD.[22] Prior characterization of these lines has been reported,[21,23] with additional data on PD-3 provided in Figure S1. Quantitative PCR (qPCR) confirmed strong upregulation of pluripotency markers (*OCT4*, *NANOG*, and *SOX2*) relative to parental lymphocytes (Figure S1A). Immunofluorescence confirmed NANOG, OCT4, SOX2, and TRA 1–60 expression in PD-3 iPSC colonies (Figure S1B). Trilineage differentiation potential of PD-3 iPSCs was assessed by qPCR for *GATA4* (endoderm), *HAND1* (mesoderm), and *TUBB3* (ectoderm) (Figure S1C), and immunofluorescence for BRAT (mesoderm), NESTIN (ectoderm), and SOX17 (endoderm) (Figure S1D), confirming successful trilineage differentiation capability. Organoid differentiation was tracked through integrated morphological, transcriptional, and immunocytochemical analyses. At days 4, 8, and 20, all lines formed spherical neuroepithelial structures (Figure 1A). Day 20 qPCR revealed robust induction of early midbrain markers, including *CNPY1A1*, *CORIN*, *EN1*, *NGN2*, *FOXA2*, *LMX1A/B*, *SHH*, *TH*, and *OTX1/2* (Figure 1B). Immunofluorescence confirmed spatial localization of midbrain identity markers: FOXA2 and LMX1A co-expression defined ventral midbrain progenitors (Figure 1C), and ZO-1 marked apical tight junctions surrounding $FOXA2^+$ rosettes (Figure 1D). By day 60, organoids expressed mature dopaminergic markers (*TH*, *NURR1* (*NR4A2*), *DDC*, *GIRK2*, *CALB1*, and *DAT*) (Figure 1E). Immunostaining confirmed TH-positive neurons co-expressing GIRK2 (a subtype-specific potassium channel), and CALB1 (calbindin) (Figure 1F), along with DDC (Dopa decarboxylase) and NFL (neurofilament light chain), indicating successful differentiation into mature midbrain dopaminergic neurons (Figure 1G).

PD-derived organoids accumulate phosphorylated and oligomeric α-synuclein

To confirm the pathological relevance of the PD-derived organoids, we analyzed the α-synuclein phosphorylation and aggregation. Western blotting at day 90 revealed a significantly elevated phosphorylated α-synuclein at Ser129 (pS129) in PD organoids versus HC, with a prominent 14 kDa band (Figures 2A and 2B). High-molecular-weight oligomers (~238 kDa and ~55 kDa), indicative of α-synuclein multimers, were detected (Figure 2C), and densitometric analysis confirmed an increased oligomeric burden (Figure 2D). Intriguingly, Syn129 immunofluorescence revealed the presence of intracellular Lewy body-like inclusions in PD organoids, recapitulating a key pathological hallmark of Parkinson's disease (Figure 2E). Tyrosine hydroxylase (TH) levels were significantly reduced in PD compared to HC, reflecting dopaminergic neuron loss (Figure 2F). These findings validate the midbrain organoids as a physiologically relevant *in vitro* model for recapitulating α-synuclein pathology characteristic of Parkinson's disease. We previously demonstrated hallmark features of PSP-RS in this system, including neurofibrillary tangles, tufted astrocytes, and gliosis,[21] further highlighting its utility as a versatile and disease-relevant model for neurodegenerative disorders.

Time-resolved miRNA profiling reveals progressive, disease-specific expression signatures

To examine dynamic miRNA changes, we performed small RNA sequencing at days 60, 90, and 120. In PSP-RS vs. HC, 142 miRNAs were upregulated and 151 downregulated at day 60; increasing to 227 and 221, respectively, by day 120 (Figure 3A). PD vs. HC showed 231 upregulated and 195 downregulated miRNAs at day 60, rising to 262 and 234 by day 120 (Figure 3B). PSP-RS vs. PD comparisons revealed increasing divergence, with 120 upregulated and 158 downregulated miRNAs at day 60, and 163 and 230 at day 120 (Figure 3C). These patterns emphasize progressive, disease-specific miRNA dysregulation. We focused on persistently upregulated miRNA across all time points, prioritizing them for their therapeutic tractability. In PSP-RS vs. HC, 69 miRNAs (23%) were consistently elevated (Figure 3D); in PD vs. HC, 102 miRNAs (30.8%) met this criterion (Figure 3E). PSP-RS vs. PD revealed 34 miRNAs (15.7%) with sustained differential expression (Figure 3F). These stable

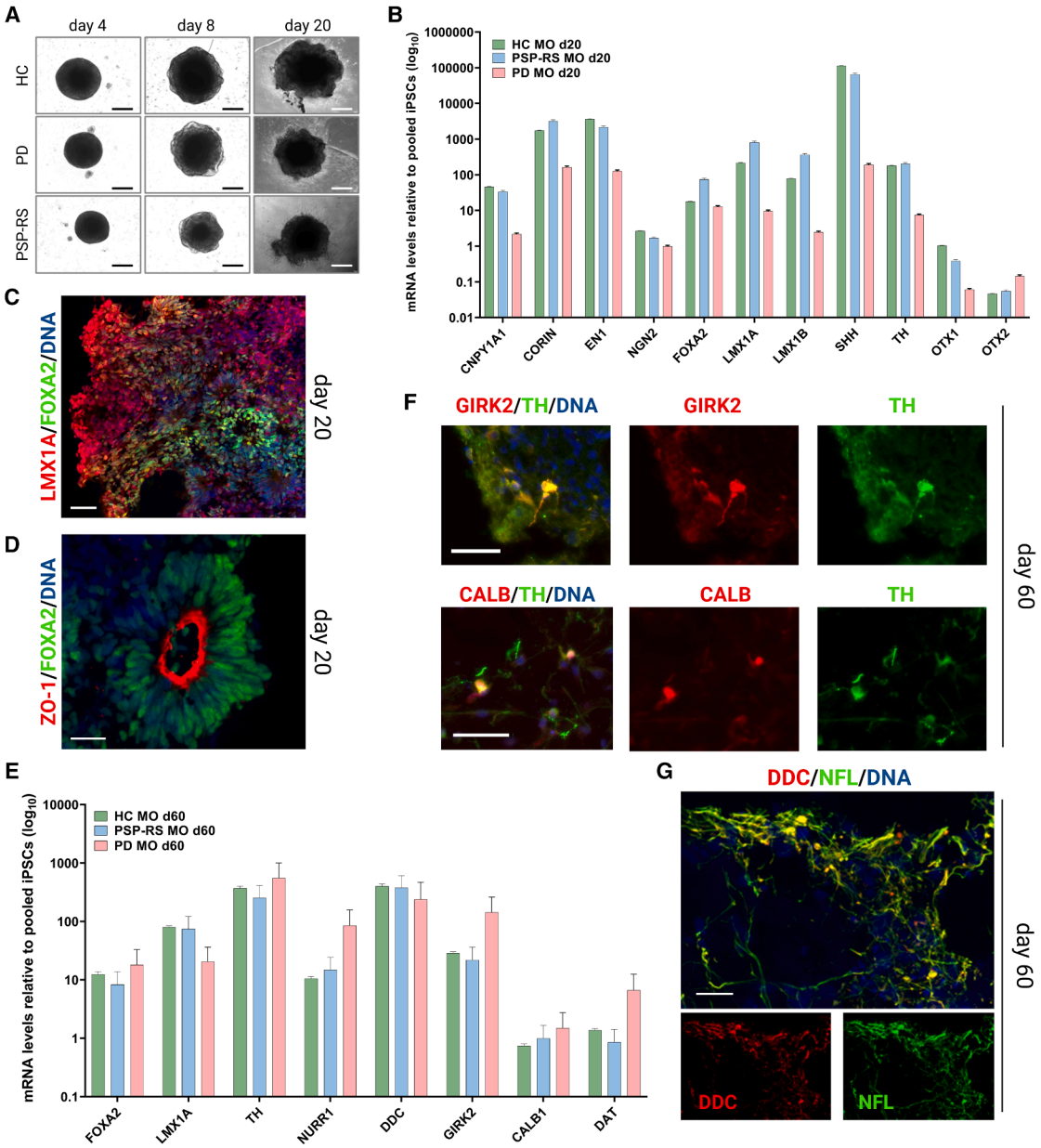

Figure 1. Generation of midbrain organoids (MOs)

(A) Representative brightfield images showing morphological development of midbrain organoids derived from healthy controls (HC), Parkinson's disease (PD), and progressive supranuclear Palsy-Richardson syndrome (PSP-RS) iPSCs at days 4, 8, and 20. Scale bars, 200 μm.

(B) Quantitative RT-PCR analysis of early midbrain progenitor markers at day 20. Data are expressed as fold change relative to pooled undifferentiated iPSCs (mean ± SEM, $n = 3$).

(C and D) Immunofluorescence staining at day 20 confirms midbrain regional identity and neuroepithelial organization, showing co-expression of FOXA2 with LMX1A (C) and ZO-1 (D). Nuclei are counterstained with DAPI (blue). Scale bars: 50 μm (C), 10 μm (D).

(E) RT-qPCR analysis of mature midbrain neuronal markers at day 60 demonstrates ongoing MO maturation across all conditions. Data are presented as fold change relative to undifferentiated iPSCs (mean ± SEM, $n = 3$).

(F) Immunofluorescence at day 60 confirms specification of dopaminergic neuronal subtypes, showing co-expression of TH with GIRK2 (A9 lineage, upper panels) and with CALB (A10 lineage, lower panels). Scale bars, 50 μm.

(G) Immunostaining for DDC (dopaminergic marker) and NFL (neuronal marker) at day 60 further validates midbrain neuronal identity. Scale bar, 50 μm. Nuclei are counterstained with DAPI (blue).

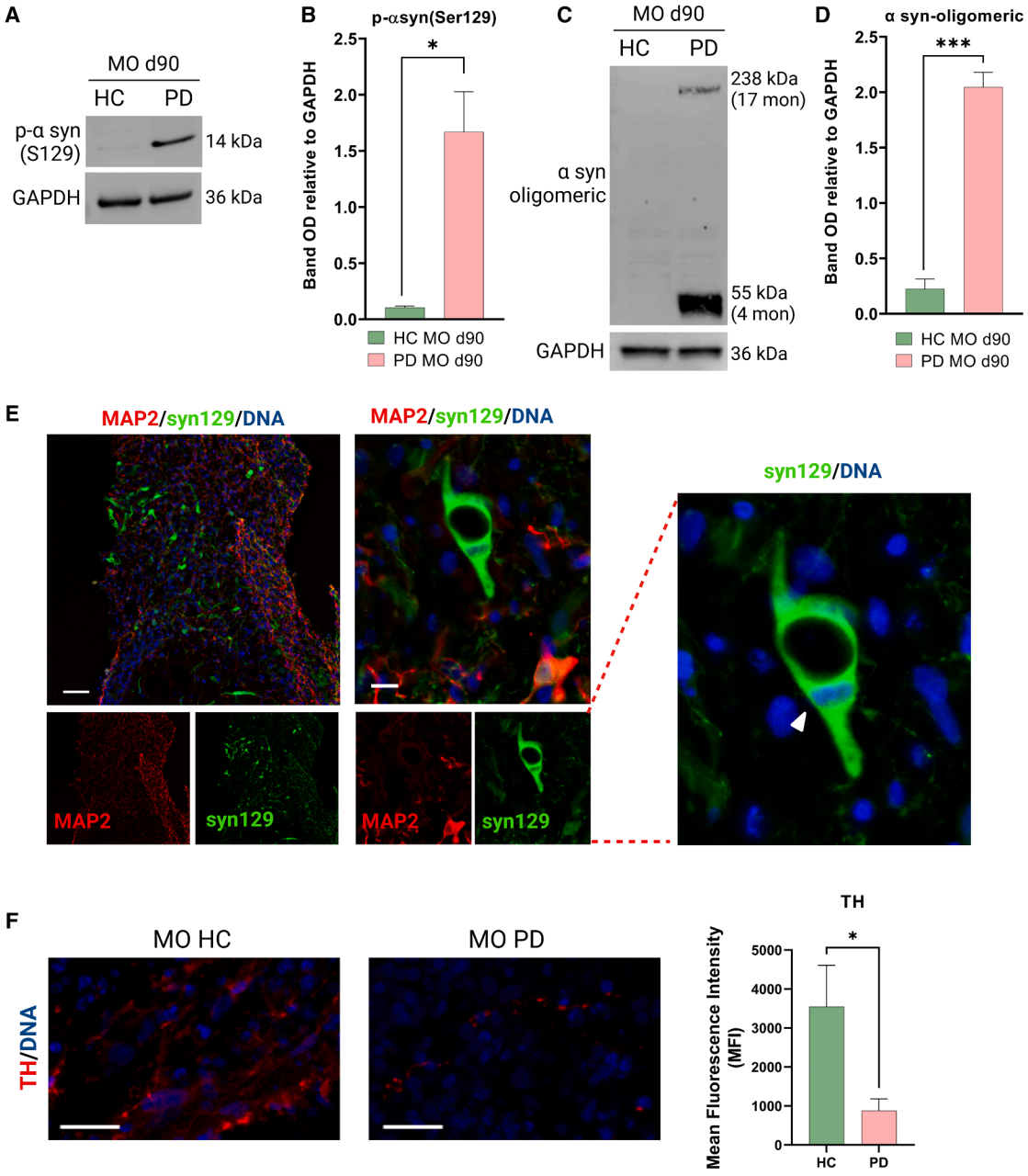

Figure 2. PD-derived MOs recapitulate hallmark pathological features

(A) Western blot analysis at day 90 reveals increased levels of phosphorylated α-synuclein at Ser129 (pS129) in PD midbrain organoids (MOs) compared to healthy controls (HC). GAPDH was used as a loading control.

(B) Densitometric quantification of pS129-α-synuclein levels normalized to GAPDH. Data are presented as mean ± SEM ($n = 3$). $p < 0.05$, Welch's t test.

(C) Immunoblot showing elevated levels of oligomeric and tetrameric α-synuclein in PD MOs relative to controls. Molecular weights are indicated for α-synuclein multimers.

(D) Quantification of oligomeric α-synuclein signal intensity normalized to GAPDH. Data represent mean ± SEM ($n = 3$). $^{**}p < 0.001$, Welch's t test.

(E) Immunofluorescence analysis of PD MO cryosections stained for MAP2 and pS129-α-synuclein reveals intracellular inclusions resembling Lewy body-like structures (white arrowhead, enlarged in right panel). Nuclei were counterstained with DAPI. Scale bars, 50 μm; 10 μm higher magnification.

(F) Immunostaining for tyrosine hydroxylase (TH) and quantification of mean fluorescence intensity (MFI) show reduced dopaminergic marker expression in PD MOs compared to HC. Data are presented as mean ± SEM from at least 12 regions of interest (ROIs) across 3 biological replicates. $p < 0.05$, Welch's t test. Scale bars, 25 μm.

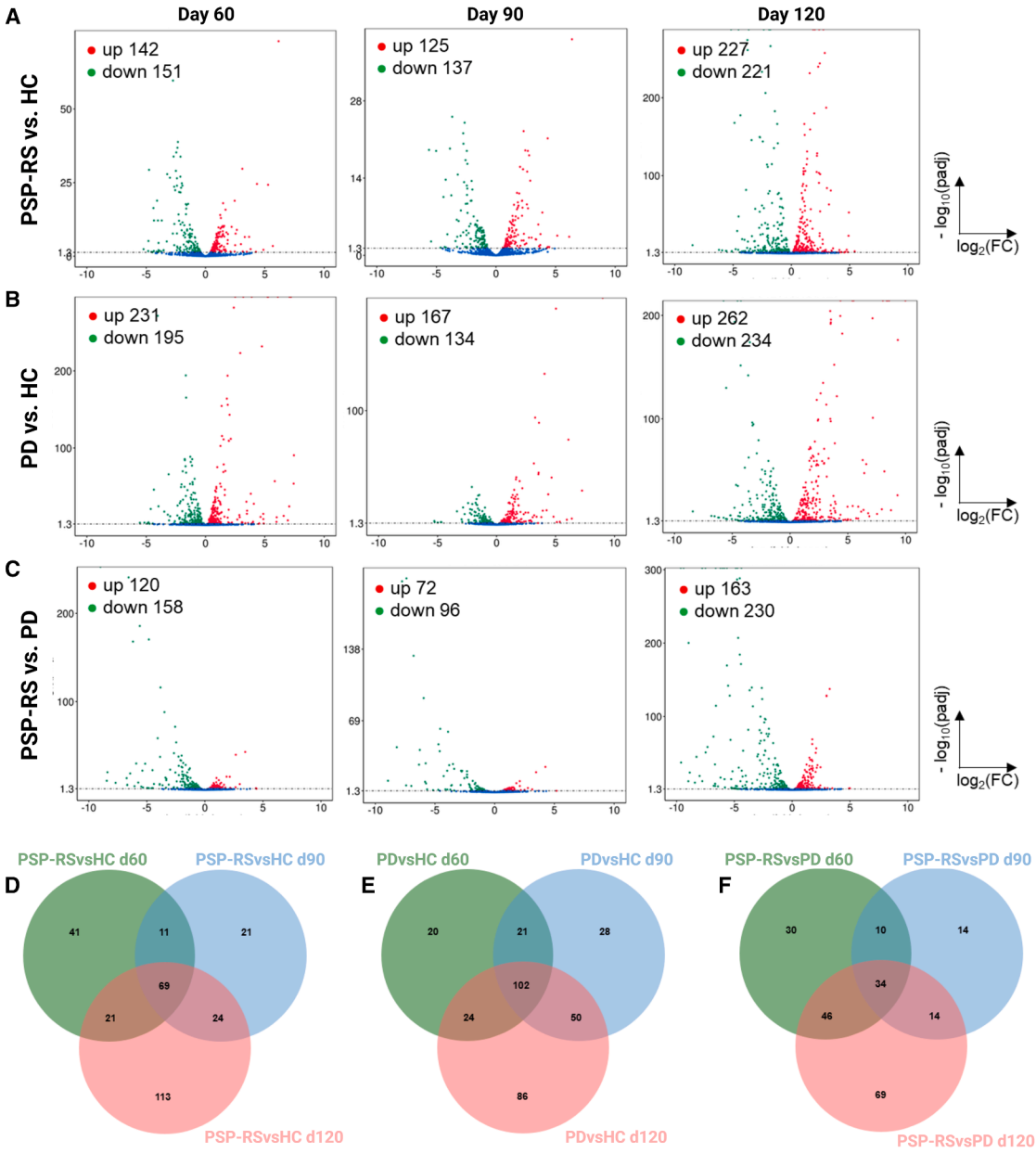

Figure 3. Differential expression of miRNAs in midbrain organoids across disease conditions and time points

(A–C) Volcano plots showing differentially expressed miRNAs at days 60, 90, and 120 for: (A) PSP-RS vs. healthy controls (HC), (B) PD vs. HC, and (C) PSP-RS vs. PD. Upregulated miRNAs (log_2 fold change >1, adjusted p value <0.05) are shown in red; downregulated miRNAs (log_2 fold change < −1, adjusted p value <0.05) are shown in green.

(D–F) Venn diagrams representing overlapping differentially expressed miRNAs across all three time points for: (D) PSP-RS vs. HC (n = 69), (E) PD vs. HC (n = 102), and (F) PSP-RS vs. PD (n = 34).

signatures were prioritized for target validation and pathways analysis. The complete list of common upregulated miRNAs is provided in Tables S3, S4, and S5.

Stable, disease-specific miRNA signatures distinguish PSP-RS and PD

To identify high-confidence candidate miRNAs, we filtered for those consistently upregulated across all three time points (day 60, 90, and 120) with average log_2 fold change >1.5. In the PSP-RS vs. HC comparison, nine miRNAs met this criterion: miR-5683, miR-3085-3p, miR-138-2-3p, miR-124-3p, miR-767-5p, miR-132-3p, miR-105-5p, miR-212-5p, and miR-129-5p (Table 1). miR-3085-3p showed the largest increase, from log_2 FC = 2.46 (day 60) to 4.75 (day 120). In PD vs. HC, 33 miRNAs were significantly upregulated, including miR-133b, miR-3120-3p, miR-214-5p, miR-199a-5p, miR-133a-5p, miR-10b-5p,

Table 1. Consistently upregulated miRNAs in PSP-RS compared to HC across all time points with log2 fold change >1.5

PSP-RS vs. HC	day 60		day 90		day 120		Average
miRNA	*log2FC*	*padj*	*log2FC*	*padj*	*log2FC*	*padj*	*log2 FC*
miR-5683	2.46	1.42e-19	2.78	7.47e-19	3.38	1.47e-81	2.88
miR-3085-3p	2.46	0.025	4.34	0.030	4.75	1.71e-05	3.85
miR-138-2-3p	1.67	0.005	2.23	2.26e-09	3.06	1.19e-84	2.32
miR-124-3p	1.59	2.06e-07	1.75	4.54e-09	2.30	1.51e-240	1.88
miR-767-5p	1.15	2.42e-08	1.41	3.50e-07	2.37	2.26e-91	1.65
miR-132-3p	1.09	1.66e-10	2.31	3.05e-23	2.39	0	1.93
miR-105-5p	1.07	2.80e-07	1.76	4.68e-12	2.36	4.07e-104	1.73
miR-212-5p	0.85	5.56e-05	1.95	6.02e-12	2.47	1.57e-102	1.76
miR-129-5p	0.63	0.005	2.45	9.50e-20	2.75	0	1.95

miR-3120-5p, miR-1-3p, miR-1245b-3p, miR-199a-3p, miR-133a-3p, miR-10b-3p, miR-143-3p, miR-145-3p, miR-143-5p, miR-193a-5p, miR-483-3p, miR-196b-5p, miR-199b-5p, miR-542-3p, miR-1299, miR-140-3p, miR-483-5p, miR-140-5p, miR-486-5p, miR-486-3p, miR-455-3p, miR-450a-5p, miR-1247-5p, miR-450b-5p, miR-455-5p, miR-212-5p, and miR-574-5p (Table 2). Comparative analysis between PSP-RS and PD identified four miRNAs selectively enriched in PSP-RS: miR-5683, miR-873-5p, miR-219a-2-3p, and miR-219b-5p (Table 3), which were subsequently prioritized for downstream target validation.

Top-ranked miRNAs and target networks define disease-specific regulatory programs

To refine disease-specific miRNA signatures, we selected the top upregulated miRNAs with the lowest adjusted *p* values from each pairwise comparison. A heatmap of TPM-normalized expression values (Figure 4A) revealed distinct sample clustering by disease group, underscoring the discriminatory capacity of the selected miRNAs. In the PSP-RS group, the most prominently upregulated miRNAs included miR-5683, miR-3085-3p, miR-138-2-3p, and miR-124-3p (Figure 4B). In contrast PD organoids exhibited increased expression of miR-1-3p, miR-133b, miR-199a-5p, and miR-10b-5p (Figure 4C); the direct comparison between PSP-RS and PD revealed selective enrichment of miR-5683, miR-873-5p, miR-219a-2-3p, and miR-219b-5p (Figure 4D). In PSP-RS organoids, miRNA target analysis revealed significant repression of *CCNB1*, *POLQ*, and *SLC7A11* (targets of miR-5683); *QPCTL* (miR-3085-3p); *REST*, *RPL7L1*, and *VPS13A* (miR-138-2-3p); and *VIM*, *SOX9*, and *CDK6* (miR-124-3p), compared to HC (Figure 4E). In PD organoids, validated repressed targets included *GJA1*, *ZNF215*, and *ZZZ3* (miR-1-3p); *HIF1A*, *ATF6*, and *GSK3B* (miR-199a-5p); *SESN3*, *CXCR4*, and *RB1CC1* (miR-133b); as well as *RPS8*, *RPS15A*, and *BRCA1* (miR-10b-5p) (Figure 4F). Direct comparison between PSP-RS and PD further highlighted confirmed selective repression of *POLQ*, *USP1*, and *HNRNPU* (miR-5683); *ZNF480*, *SPB1*, and *CANX* (miR-219b-5p); *CDK3*, *EN2*, and *ADAR* (miR-873-5p); and *CCNE2*, *SESN3*, and *CDK6* (miR-219a-2-3p) (Figure 4G). To validate the robustness of these miRNA signatures identified in pooled midbrain organoids, we examined their expression patterns in individual organoids derived from single iPSCs lines (PSP-RS-1, PD-1, and HC-1). Consistent with pooled data, miR-5683, miR-3085-3p, miR-138-2-3p, and miR-124-3p were significantly upregulated in PSP-RS-1 organoids relative to HC-1 (Figure S2A). Similarly, miR-1-3p and miR-10b-5p were elevated in PD-1 compared to HC-1 (Figure S2B). The PSP-RS-1 vs. PD-1 comparisons confirmed significantly higher expression of miR-5683, miR-219b-5p, miR-873-5p, and miR-219a-2-3p in PSP-RS organoids (Figure S2C). We next assessed expression of selected miRNA target genes, as identified via integrative target prediction and pathway enrichment. In PSP-RS-1 organoids, target genes including *CCNB1* and *POLQ* (miR-5683), *QPCTL* (miR-3085-3P), *RPL7L1* and *VPS13A* (miR-138-2-3p), *SOX9* and *CDK6* (miR-124-3p) were significantly downregulated relative to HC-1 (Figure S2D). In PD-1, targets such as *GJA1* and *ZNF215* (miR-1-3p), *RPS15A*, and *BRCA1* (miR-10b-5p) showed reduced expression compared to HC-1 (Figure S2E). Comparison of PSP-RS-1 and PD-1 revealed selective downregulation of *POLQ* and *USP1* (miR-5683), *EN2* and *ADAR* (miR-873-5p), *ZNF480*, and *SPB1* (miR-219b-5p), *CDK6* and *SESN3* (miR-219a-2-3p) in PSP-RS-1 (Figure S2F).

Gene ontology analysis of selected miRNA target genes

To investigate the biological relevance of candidate miRNAs, we performed gene ontology (GO) enrichment analysis on their predicted target genes to identify associated pathways and functional categories. Enrichment profiles were generated for each comparison PSP-RS vs. HC (Figure S3A), PD vs. HC (Figure S3B), and PSP-RS vs. PD (Figure S3C) to identify distinct functional pathways associated with disease-specific miRNA targets. To further refine mechanistic insights, we performed individual GO enrichment analyses for each candidate miRNA, enabling the identification of miRNA-specific functional signatures. In PSP-RS, miR-5683 and miR-124-3p targets were enriched in pathways related to synaptic organization, cytoskeletal remodeling, organelle fission, spindle microtubule attachment to kinetochores, and chromosome segregation (Figure 5A). While some of these functions are associated with mitosis, they may reflect disruptions in glial or progenitor dynamics relevant to PSP pathology. In PD, targets of miR-133b, miR-199a-5p, miR-10b-5p, and miR-1-3p were enriched in pathways linked to synaptic function, mitochondrial homeostasis, and oxidative stress response, hallmarks feature of α-synuclein pathology

Table 2. Consistently upregulated miRNAs in PD compared to HC across all time points with log2 fold change >1.5

PD vs. HC	day 60		day 90		day 120		Average
miRNA	*log2FC*	*padj*	*log2FC*	*padj*	*log2FC*	*padj*	*log2FC*
miR-133b	7.25	1.40e-30	7.43	1.95e-54	9.33	5.85e-177	12.00
miR-3120-3p	4.38	2.52e-27	7.06	7.72e-25	8.17	7.76e-50	6.54
miR-214-5p	4.38	2.52e-27	7.05	7.83e-25	8.17	7.76e-50	6.54
miR-199a-5p	4.06	4.72e-133	7.08	0	8.36	0	6.50
miR-133a-5p	4.83	1.04e-07	4.87	3.48e-15	9.30	9.01e-27	6.34
miR-10b-5p	3.16	2.06e-54	7.19	0	8.57	0	6.31
miR-3120-5p	3.39	1.14e-07	6.59	1.56e-12	8.74	2.65e-12	6.24
miR-1-3p	5.03	3.15e-190	5.22	0	8.42	0	6.22
miR-1245b-3p	5.36	0.003	5.98	8.62e-05	6.86	1.90e-06	6.07
miR-199a-3p	3.60	4.39e-90	6.10	0	8.03	0	5.91
miR-133a-3p	0.67	0.036	4.75	1.54e-232	7.14	6.45e-198	4.17
miR-10b-3p	2.47	0.001	6.00	1.03e-10	7.94	3.22e-13	5.47
miR-143-3p	3.54	6.34e-45	5.28	0	6.42	3.43e-48	5.08
miR-145-3p	2.81	0.0003	4.87	2.49e-08	6.76	1.93e-09	4.82
miR-143-5p	3.19	6.14e-09	2.37	2.91e-11	5.42	2.32e-16	3.66
miR-193a-5p	2.06	2.55e-05	4.07	2.75e-28	6.60	6.88e-57	4.25
miR-483-3p	2.30	6.66e-10	3.44	6.11e-31	6.29	8.34e-61	4.01
miR-196b-5p	2.97	0.0025	3.89	0.0074	3.90	0.0014	3.59
miR-199b-5p	2.18	1.19e-32	3.18	0	5.39	0	3.58
miR-542-3p	1.64	1.94e-40	2.50	0	5.50	0	3.21
miR-1299	2.67	2.86e-11	2.88	7.76e-11	3.89	1.59e-20	3.15
miR-140-3p	1.08	4.22e-20	3.90	0	4.36	0	3.11
miR-483-5p	2.10	1.07e-05	2.68	8.04e-08	3.95	1.69e-18	2.91
miR-140-5p	0.88	1.12e-06	2.93	6.73e-224	4.52	4.18e-183	2.78
miR-486-5p	1.86	7.95e-18	1.97	7.79e-110	3.54	1.15e-196	2.46
miR-486-3p	1.87	1.79e-17	1.96	4.10e-110	3.53	6.35e-194	2.45
miR-455-3p	0.86	0.0001	2.13	1.60e-112	3.48	6.42e-205	2.16
miR-450a-5p	1.13	8.59e-07	1.35	2.32e-17	3.52	2.86e-98	2.00
miR-1247-5p	1.14	0.010	1.92	0.0003	2.60	4.96e-05	1.89
miR-450b-5p	0.80	3.23e-09	1.23	1.95e-54	3.51	1.32e-192	1.85
miR-455-5p	0.94	6.11e-10	1.80	1.08e-164	2.64	2.39e-125	1.79
miR-212-5p	0.49	0.037	1.63	1.40e-46	2.78	7.93e-60	1.63
miR-574-5p	0.44	0.027	0.96	3.06e-18	3.14	1.93e-114	1.51

(Figure 5B). In the PSP-RS vs. PD comparison, miR-219a-2-3p and miR-219b-5p targets were associated with mRNA transport, p53 signaling, and glycosyltransferase activity (Figure 5C). miR-5683 emerged as a consistently enriched and discriminatory miRNA across all comparisons, reinforcing its biomarker potential. miRNAs without validated targets or significant enrichment (*e.g.*, miR-3085-3p, miR-138-2-3p, and miR-873-5p) were excluded from GO analysis. To further investigate the relevance of disease-associated miRNAs, we performed KEGG (Kyoto Encyclopedia of Genes and Genomes) pathway enrichment analysis on their predicted targets (Figure S4). In PSP-RS organoids, miR-124-3p was linked to pathways involved in intracellular signaling and cytoskeletal dynamics, including PI3K-Akt, MAPK, Ras, and Rap1 signaling (Figure S4A). In PD organoids, miR-1-3p and miR-133b enriched similar signaling pathways, with additional involvement in dopaminergic synapse and JAK-STAT signaling (Figures S4B and S4C). miR-199a-5p and miR-10b-5p were associated with apoptosis, cellular senescence, and p53 signaling (Figures S4D and S4E), underscoring stress-related mechanisms in PD. Notably, miR-219a-2-3p, differentially expressed in PSP-RS versus PD, selectively enriched the p53 pathway (Figure S4F), suggesting a disease-specific regulatory role. These analyses reveal both shared and distinct miRNA-driven pathway alterations in PSP-RS and PD.

Dysregulation of oxidative stress, mitochondrial dynamics, and apoptosis in PSP-RS and PD organoids

To link miRNA profiles to functional outcomes, we examined expression of genes and proteins involved in oxidative stress, mitochondrial dynamics, and apoptosis in midbrain organoids.

Table 3. Consistently upregulated miRNAs in PSP-RS compared to PD across all time points with log2 fold change >1.5

PSP-RS vs. PD	day 60		day 90		day 120		Average
miRNA	*log2FC*	*padj*	*log2FC*	*padj*	*log2FC*	*padj*	*log2FC*
miR-5683	1.87	1.14e-15	2.10	2.00e-11	2.45	1.43e-31	2.14
miR-873-5p	1.31	1.09e-07	1.82	1.94e-09	2.03	3.42e-51	1.72
miR-219b-5p	0.76	1.93e-08	1.24	4.74e-05	2.97	1.64e-128	1.66
miR-219a-2-3p	0.76	1.91e-08	1.24	4.74e-05	2.98	3.38e-129	1.66

qPCR revealed disease-specific alterations in antioxidant gene expression. In PSP-RS organoids, *SOD2* and *GPX1* were downregulated, while *NRF2* expression remained unchanged. In contrast, PD organoids exhibited significant downregulation of *SOD2*, *GPX1*, and *NRF2*, suggesting a more extensive disruption of the antioxidant defense pathway (Figure 6A). Oxidative stress was further evaluated at the protein level, with particular focus on NRF2, a master regulator of the antioxidant response. NRF2 expression was consistently reduced in both PD and PSP-RS organoids compared to HC (Figures 6B and S5A). Mitochondrial dynamics were also disrupted. PSP-RS organoids displayed reduced expression of MFN2, FIS1, OPA1, and DRP1, indicative of impaired mitochondrial fusion and fission processes. In contrast, PD organoids showed increased levels of MFN1, FIS1, and DRP1 alongside decreased OPA1, consistent with a shift toward enhanced mitochondrial fragmentation (Figure 6C). To further confirm mitochondrial dysfunction, we assessed the expression of PGC-1α and NDUFS1, key regulators of mitochondrial biogenesis and electron transport chain activity, respectively. Both proteins were significantly downregulated in PD and PSP-RS compared to HC; conversely, PARKIN, an E3 ubiquitin ligase essential for mitochondrial quality control through mitophagy,[24] was significantly upregulated in both PD and PSP-RS compared to HC (Figures 6D and S5B). In parallel, mitochondrial morphology was quantitatively assessed by immunostaining for TOM20, followed by image-based analysis using validated protocol for mitochondrial morphometric profiling.[25] This analysis revealed a marked increase in mitochondrial puncta and a concomitant reduction in elongated, interconnected networks in both disease groups, indicative of disrupted mitochondrial dynamics (Figure 6E). To investigate whether these alterations were associated with apoptotic signaling, we examined the expression of pro-apoptotic markers. *BAX* and *FAS*, along with stress-responsive genes *CELF2* and *PEG3*, were significantly upregulated in PD organoids (Figure S5C), suggesting activation of apoptotic and cellular stress pathways. Similar results were previously shown in PSP-RS organoids.[21] Apoptotic dysregulation was further confirmed at the protein level, with elevated expression of the pro-apoptotic marker BAX and reduced levels of the anti-apoptotic protein BCL-XL in both PSP-RS and PD organoids relative to HC (Figures 6F and S5D). These findings were corroborated by TUNEL assay, which revealed a significant increase in apoptotic cells in both disease groups, with PD displaying the highest proportion of TUNEL-positive cells ($p < 0.01$) (Figure 6G). Together, these results suggest that miRNA-mediated regulatory networks converge on key cellular oxidative pathways, namely oxidative stress, mitochondrial dysfunction, and apoptosis, in a disease-specific manner.

DISCUSSION

Although PSP-RS and PD share overlapping early clinical presentations, they are biologically distinct neurodegenerative disorders. PD is primarily associated with α-synuclein aggregation and dopaminergic neurodegeneration, while PSP-RS is marked by widespread deposition of hyperphosphorylated tau in the brainstem and basal ganglia regions.[5] This symptomatic overlap often delays accurate diagnosis and hampers early therapeutic intervention. Consequently, the identification of molecular biomarkers capable of distinguishing PD and PSP-RS at prodromal stages remains a critical unmet clinical need. Consequently, the identification of molecular biomarkers that can reliably distinguish between PD and PSP-RS, particularly at prodromal stages, remains a critical unmet clinical need. MicroRNAs (miRNAs), which regulate gene expression post-transcriptionally, have emerged as promising candidates for biomarker discovery in neurodegeneration.[26] Dysregulated miRNAs are known to influence neuroinflammation, synaptic function, mitochondrial dynamics, and apoptosis.[27–29] However, most miRNA studies to date rely on peripheral fluids, which may not accurately reflect the central nervous system (CNS) molecular landscape, particularly in early disease.[16] To address this gap, we employed iPSC-derived midbrain organoids as a physiologically relevant 3D model of PD and PSP-RS. These organoids recapitulate key aspects of midbrain architecture and neuropathology, including the presence of dopaminergic neurons, glial cell populations, and hallmark proteinopathies such as α-synuclein inclusions and tau tangles.[19,30,31] Importantly, the use of iPSC-derived midbrain organoids provides a human, three-dimensional neural model that enables the investigation of miRNA signatures within a disease-intrinsic and CNS-relevant context. This system supports longitudinal miRNA profiling under controlled experimental conditions, allowing the capture of molecular alterations directly associated with neuronal pathology while minimizing confounding influences from systemic factors, such as peripheral inflammation, age-related comorbidities, or medication exposure. To enhance the robustness of miRNA signal detection and mitigate batch-specific technical variability, we employed a donor-pooling strategy whereby iPSC lines from multiple donors within each group (PSP-RS, PD, and healthy controls) were combined prior to organoids differentiation. While this approach may obscure individual-specific variability, it facilitates the identification of convergent, disease-associated miRNA signatures that are reproducibly observed across genetically diverse backgrounds. This strategy is consistent with recent organoid-based transcriptomic frameworks, such as the study by Bolaños et al.,[22] which

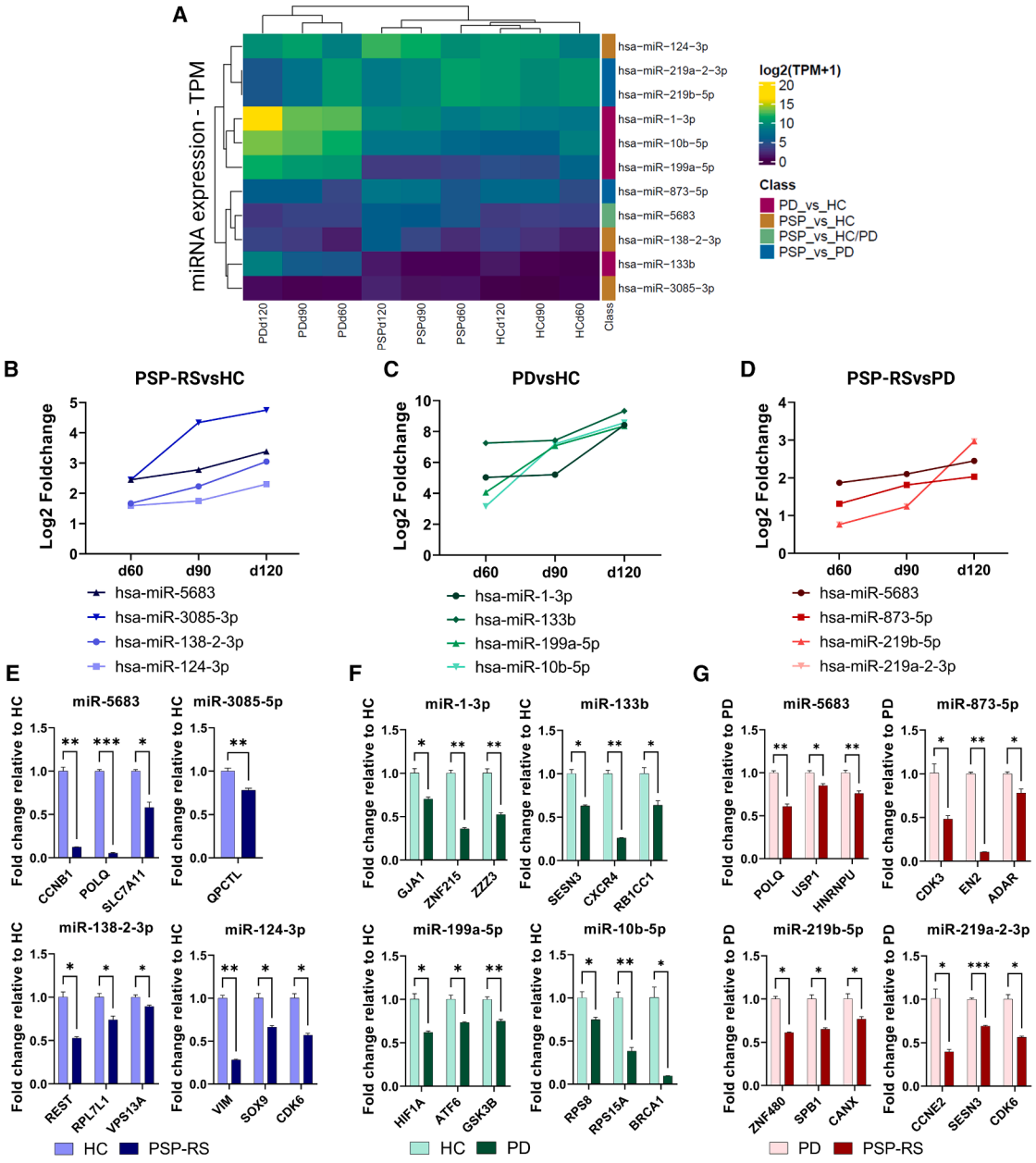

Figure 4. Identification and validation of differentially expressed miRNAs and their predicted target genes

(A) Heatmap displaying the expression profiles (TPM: transcripts per million) of selected differentially expressed miRNAs across healthy control (HC), Parkinson's disease (PD), and PSP-Richardson syndrome (PSP-RS) midbrain organoids at different time points. Unsupervised clustering reveals disease- and condition-specific miRNA expression patterns.

(B–D) Temporal expression trends of representative miRNAs in: (B) PSP-RS vs. HC, (C) PD vs. HC, (D) PSP-RS vs. PD. Expression values are shown as $\log_2$ fold change at days 60, 90, and 120.

(E–G) RT-qPCR validation of predicted target genes of selected differentially expressed miRNAs: (E) PSP-RS vs. HC, (F) PD vs. HC, (G) PSP-RS vs. PD. Bar graphs represent fold changes in gene expression relative to controls. Data are shown as mean ± SEM (n = 3). Statistical significance: $^{*}p < 0.05$, $^{**}p < 0.01$, $^{***}p < 0.001$; Welch's t-test.

demonstrated that pooled differentiations yield reproducibility and cell-type specific molecular profiles. Our results uncovered temporally stable, disease-specific miRNA signatures that robustly differentiate PSP-RS from PD and from healthy controls. Notably, PSP-RS organoids exhibited consistent upregulation of miR-5683, miR-3085-3p, miR-138-2-3p, and miR-124-3p compared to control, and miR-5683, miR-873-5p, miR-219a-2-3p, and miR-219b-5p, compared to PD organoids. In

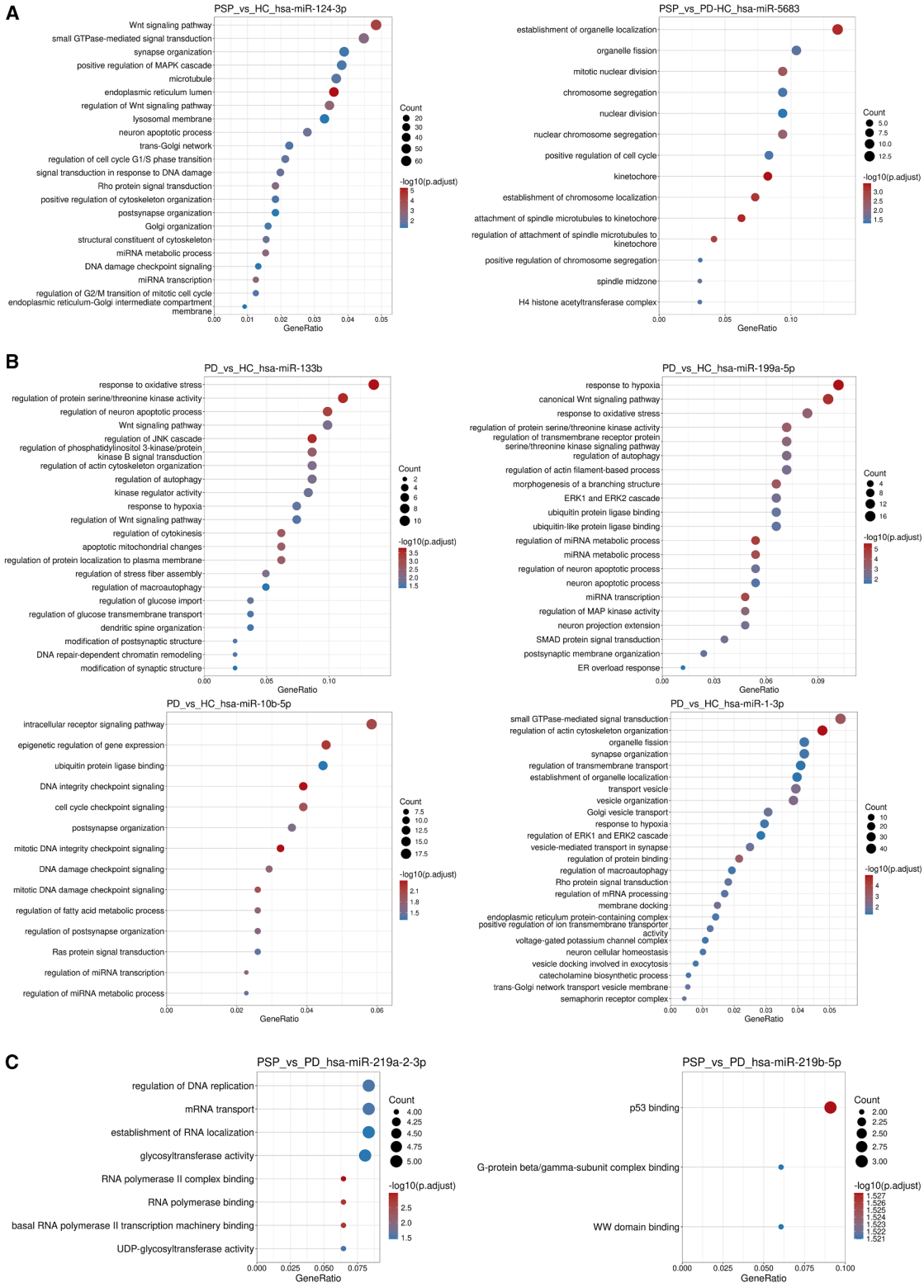

Figure 5. Gene ontology (GO) enrichment analysis of predicted target genes of differentially expressed miRNAs

(A) GO enrichment analysis of target genes for miR-124-3p (left) and miR-5683 (right), showing significantly enriched biological processes in PSP-RS vs. HC and PSP-RS vs. PD comparisons, respectively.

(legend continued on next page)

contrast, PD organoids showed increased expression of miR-1-3p, miR-133b, miR-10b-5p, and miR-199a-5p. These distinct miRNA profiles align with the molecular pathologies of their respective diseases. Gene ontology (GO) enrichment analysis of validated targets revealed divergent regulatory networks. In PSP-RS, dysregulated miRNAs were associated with cytoskeletal remodeling, mitotic spindle organization, and chromosome segregation—hallmarks of tau-induced microtubule instability and aberrant activation of cell cycle pathways in postmitotic neurons. Specifically, miR-124-3p and miR-5683 regulated targets involved in mitotic control and organelle dynamics,[32] supporting their functional relevance in PSP-RS. In contrast, PD-associated miRNAs targeted genes linked to synaptic signaling, mitochondrial homeostasis, and oxidative stress—core processes affected by α-synuclein toxicity. For example, miR-133b, miR-10b-5p, and miR-199a-5p modulated pathways involving ERK/JNK signaling, glucose metabolism, and proteostasis, all implicated in PD pathogenesis. These findings are consistent with prior reports linking these miRNAs to dopaminergic dysfunction and neuronal stress responses. Among the differentially expressed miRNAs, the miR-219 family (miR-219a-2-3p and miR-219b-5p) emerged as robust PSP-RS-specific markers. These miRNAs regulate genes involved in mRNA transport, glycosylation, and p53 signaling,[33,34] suggesting roles in transcriptional homeostasis and neuronal integrity. Their selective upregulation in PSP-RS organoids and repression of targets, such as *ZNF480*, *CANX*, and *SPB1* implicate them in disease-specific regulatory programs.[5] Several of the top miRNA signatures identified in midbrain organoids align with previously reported clinical data from plasma or cerebrospinal fluid (CSF) studies, underscoring their potential translational relevance. For example, elevated plasma levels of miR-133b have been reported in early-stage PD patients.[35] Notably, miR-133b is enriched in midbrain dopaminergic neurons and plays a critical role in their differentiation and maintenance.[36] Its upregulation in PD organoids may therefore reflect pre-dendritic, compensatory changes aimed at preserving neuronal identity and function. Similarly, miR-1-3p, which has been reported as downregulated in whole blood of *de novo* PD patients but upregulated in early-onset PD,[37] showed increased expression in our PD organoids. This apparent dual behavior may reflect stage-specific regulation, with our model capturing early, preclinical disease states. In the context of PSP-RS, miR-873-3p has been found significantly elevated in the CSF of PSP patients from early to advanced disease stage.[38] Correspondingly, our PSP-RS organoids showed upregulation of the complementary strand, miR-873-5p, suggesting that dysregulation of the miR-873 duplex may represent an early, intrinsic molecular hallmark of tauopathy. Beyond the top four miRNAs highlighted in each comparison, we also identified several additional miRNAs that were consistently upregulated across days 60, 90, and 120 of differentiation and are supported by independent clinical evidence (Tables 1, 2, and 3). For instance, miR-214, significantly upregulated in serum of individuals with prodromal PD compared to both healthy controls and patients with advanced disease,[39] was consistently elevated in our PD organoids, suggesting a role in early pathophysiological responses preceding neurodegeneration. Similarly, miR-145-3p, previously found elevated in the saliva of PD patients,[40] was also upregulated in PD organoids, reinforcing its potential as non-invasive biomarker detectable both centrally and peripherally. In PSP-RS organoids, miR-138, implicated in tau pathology (phosphorylation and aggregation) and previously shown to be upregulated in Alzheimer's disease brain tissues,[41] was significantly elevated, suggesting conserved pathogenic roles across tauopathies. Collectively, these convergences between organoids derived and circulating miRNA signatures support the translational relevance of our findings and suggest that select miRNAs may serve as stable, disease-relevant biomarkers that originate from CNS pathology yet are accessible through peripheral biofluids. Although the primary aim of this study was not a comprehensive molecular characterization, we performed targeted validation to begin linking disease-specific miRNA signatures to functional outcomes. We investigated key stress-response pathways in midbrain organoids, focusing on mitochondrial homeostasis, redox balance, and programmed cell death. PSP-RS organoids exhibited clear signs of mitochondrial instability and impaired oxidative resilience, while PD organoids showed broader dysregulation, characterized by heightened oxidative stress and increased apoptotic susceptibility. These phenotypes were corroborated by TUNEL assays, which revealed elevated apoptosis in both disease models, with a more pronounced burden in PD. Together, these findings suggest that distinct miRNA regulatory networks drive disease-specific molecular cascades converging on mitochondrial dysfunction and cell death. Our results nominate select miRNAs as promising candidates for further validation in patient cohorts and underscore the utility of iPSC-derived midbrain organoids as a physiologically relevant platform for dissecting neurodegenerative mechanisms and discovering CNS-specific biomarkers.

Limitations of the study

To establish the clinical relevance of our findings, validation in larger, independent patient cohorts—including both peripheral biofluids and CNS-derived specimens such as cerebrospinal fluid and postmortem brain tissue—is essential. Furthermore, current midbrain organoid systems lack key cellular components, such as microglia and vasculature, and incompletely model mature neuronal circuitry. Future iterations incorporating vascularization and co-culture systems will enhance physiological fidelity. Finally, functional interrogation of candidate miRNAs

(B) GO analysis of predicted targets for miR-133b, miR-199a-5p, miR-10b-5p, and miR-1-3p, differentially expressed in PD vs. HC comparisons, highlighting key pathways related to oxidative stress, neuronal apoptosis, autophagy, and synaptic organization.
(C) GO terms enriched among predicted targets of miR-219a-2-3p and miR-219b-5p, which were differentially expressed in PSP-RS vs. PD. Enriched terms include RNA processing, transcription regulation, and protein binding functions. Each dot represents a significantly enriched GO term, with dot size indicating the number of genes (Count) associated with the term and color representing the adjusted *p* value ($\log_{10}$ *padj*). GeneRatio refers to the proportion of target genes associated with a given GO term.

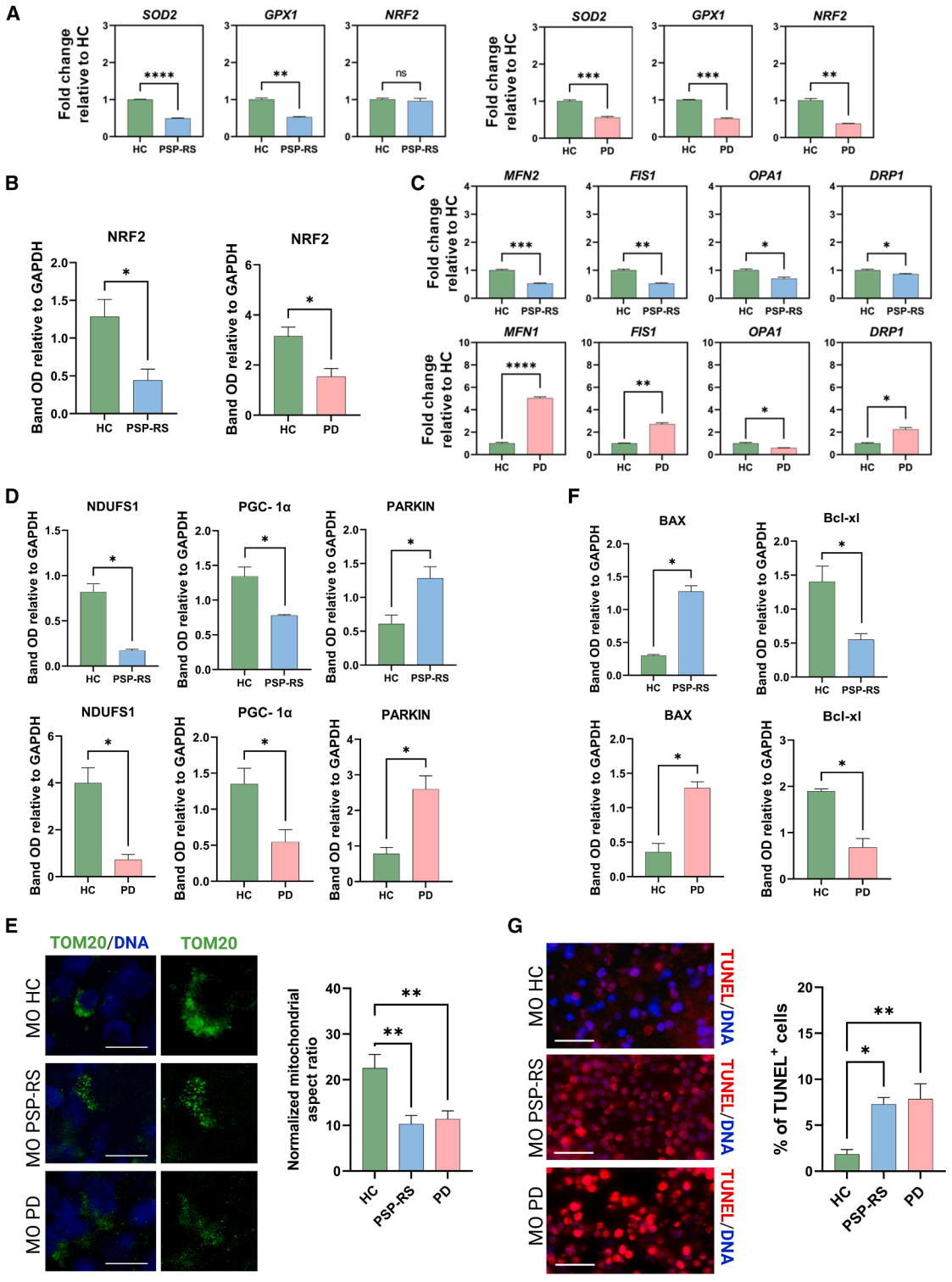

Figure 6. Mitochondrial dysfunction, oxidative stress, and DNA damage response impairments in PD and PSP-RS midbrain organoids

(A) RT-qPCR analysis of oxidative stress response genes (*SOD2*, *GPX1*, and *NRF2*) in PSP-RS and PD organoids compared to healthy controls (HC).

(B) Western blot quantification of NRF2 expression in PD and PSP-RS patient-derived samples relative to healthy controls.

(C) Expression of genes involved in mitochondrial dynamics (MFN2, FIS1, OPA1, and DRP1) in PSP-RS and PD organoids vs. HC.

(D) Western blot quantification of NDUFS1, PGC-1α, and PARKIN expression in PD and PSP-RS patient-derived samples relative to healthy controls.

(legend continued on next page)

using tools, such as antagomirs or CRISPR-based knockout strategies will be critical to delineate their causal roles in PSP-RS and PD pathogenesis.

RESOURCE AVAILABILITY

Lead contact

Additional information and data are available from the lead contact, Dr. Elvira Immacolata Parrotta (parrotta@unicz.it) upon reasonable request.

Materials availability

Requests for materials and reagents should also be directed to the lead contact, Dr. Elvira Immacolata Parrotta (parrotta@unicz.it).

Data and code availability

- **Data**: the sRNA-seq data discussed in this paper have been deposited in NCBI's Gene Expression Omnibus[42] and are accessible through GEO Series accession number GSE294029 (https://www.ncbi.nlm.nih.gov/geo/query/acc.cgi?acc=GSE294029), as reported in the key resources table.
- **Code**: this paper does not report original code.
- **Additional information**: further details needed to replicate the analyses presented in this study can be obtained from the lead contact Dr. Elvira Immacolata Parrotta (parrotta@unicz.it) upon request.

ACKNOWLEDGMENTS

We are grateful to the donors of these studies, without which this work would not have been possible. This work was supported by the following fundings: PNRR Project # CN00000041: National Center for Gene Therapy and Drugs Based on RNA Technology (CN RNA & Gene Therapy) CUP J33C22001130001 to G.C. and G.P. PNRR project: A multiscale integrated approach to the study of the nervous system in health and disease (MNESYS) CUP D33C22001340002 to G.C. and G.P. INNOVA—Italian network of excellence for advanced diagnosis (PNC-EJ-2022-23683266 PNC-HLS-DA) to G.P. This work was also supported by ELIXIR-IT through the empowering project ELIXIRNextGenIT (grant code IR0000010 to G.P.).

AUTHOR CONTRIBUTIONS

E.I.P. and G.C. conceived and designed the study. D.V., C.Z., S.S., V.L., G.L. B., M.G.T., and I.L. performed the experiments. D.V., C.Z., and S.S. conducted data analysis. D.V., C.Z., S.S., and D.B. generated the figures; D.B., F.C., E.F., and G.P. carried out the bioinformatics analyses. Andrea Quattrone and Aldo Quattrone were responsible for patient recruitment and provided clinical samples and data. E.I.P. and G.C. wrote the manuscript. All authors reviewed and approved the final version of the manuscript.

DECLARATION OF INTERESTS

The authors declare no competing interests.

DECLARATION OF GENERATIVE AI AND AI-ASSISTED TECHNOLOGIES IN THE WRITING PROCESS

During the preparation of this work, the author(s) used ChatGPT in order to assist with English language editing. After using this tool or service, the author(s) reviewed and edited the content as needed and take(s) full responsibility for the content of the publication.

STAR★METHODS

Detailed methods are provided in the online version of this paper and include the following:

- KEY RESOURCES TABLE
- EXPERIMENTAL MODEL AND STUDY PARTICIPANT DETAILS
- METHOD DETAILS
  - Generation of PD patient-induced pluripotent stem cells (iPSCs)
  - Generation of midbrain organoids (MOs)
  - RNA extraction, reverse transcription, and quantitative real-time PCR
  - Immunofluorescence
  - Protein extraction and immunoblotting
- QUANTIFICATION AND STATISTICAL ANALYSIS
  - miRNA sequencing
  - Bioinformatics analysis
  - GO enrichment analysis

SUPPLEMENTAL INFORMATION

Supplemental information can be found online at https://doi.org/10.1016/j.isci.2025.113162.

Received: April 14, 2025
Revised: July 10, 2025
Accepted: July 15, 2025
Published: July 18, 2025

REFERENCES

1. Owolabi, L. (2013). Progressive supranuclear palsy misdiagnosed as Parkinson's disease: a case report and review of literature. Ann. Med. Health Sci. Res. *3*, S44–S47. https://doi.org/10.4103/2141-9248.121221.
2. Stein, Z.L.-G. (1985). Parkinson's Disease and Progressive Supranuclear Palsy. Arch. Intern. Med. *145*, 952. https://doi.org/10.1001/archinte.1985.00360050222047.
3. Obeso, J.A., Stamelou, M., Goetz, C.G., Poewe, W., Lang, A.E., Weintraub, D., Burn, D., Halliday, G.M., Bezard, E., Przedborski, S., et al. (2017). Past, Present, and Future of Parkinson's Disease: A Special Essay on the 200th Anniversary of the Shaking Palsy. Mov. Disord. *32*, 1264–1310. https://doi.org/10.1002/mds.27115.
4. Grazia, S.M., and Goedert, M. (2018). Neurodegeneration and the ordered assemblymof α-synuclein. Cell Tissue Res. *373*, 137–148. https://doi.org/10.1007/s00441-017-2706-9.
5. Stamelou, M., de Silva, R., Arias-Carrión, O., Boura, E., Höllerhage, M., Oertel, W.H., Ulrich, M., and Höglinger, G.U. (2010). Rational therapeutic approaches to progressive supranuclear palsy. Brain *133*, 1578–1590. https://doi.org/10.1093/brain/awq115.
6. Dickson, D.W. (2012). Parkinson's disease and parkinsonism: neuropathology. Cold Spring Harb. Perspect. Med. *2*, a009258. https://doi.org/10.1101/cshperspect.a009258.
7. Bartel, D.P. (2009). MicroRNAs: target recognition and regulatory funcions. Cell *136*, 215–233. https://doi.org/10.1016/j.cell.2009.01.002.

(E) Representative images of TOM20 immunofluorescence and quantification of mitochondrial morphology, showing mitochondrial puncta and interconnected networks expressed as normalized mitochondrial aspect ratio. At least 10 ROI were analyzed for each condition. Scale bar 10 μm (F) Elevated expression of the pro-apoptotic protein BAX and reduced levels of the anti-apoptotic protein BCL-XL in patient-derived samples compared to HC.
(G) Representative TUNEL staining images and quantification showing increased apoptosis in PD and PSP-RS organoids vs. HC. Nuclei counterstained with DAPI (blue). Scale bar, 25 μm. Quantification based on manual counting of at least 10,000 cells per condition. All data are presented as mean ± SEM from three biological replicates. Statistical significance: ns = not significant; $p < 0.05$, $p < 0.01$, $^{*}p < 0.001$, $^{**}p < 0.0001$. Welch's t test was used unless otherwise specified; Tukey's one-way ANOVA test was applied for (E) and (G).

8. Ha, M., and Kim, V.N. (2014). Regulation of microRNA biogenesis. Nat. Rev. Mol. Cell Biol. *15*, 509–524. https://doi.org/10.1038/nrm3838.

9. Lau, P., and de Strooper, B. (2010). Dysregulated microRNAs in neurodegenerative disorders. Semin. Cell Dev. Biol. *21*, 768–773. https://doi.org/10.1016/j.semcdb.2010.01.009.

10. Lusardi, T.A., Phillips, J.I., Wiedrick, J.T., Harrington, C.A., Lind, B., Lapidus, J.A., Quinn, J.F., and Saugstad, J.A. (2017). MicroRNAs in Humand Cerebrospinal Fluid as Biomarkers for Alzheimer's Disease. J. Alzheimers Dis. *55*, 1223–1233. https://doi.org/10.3233/JAD-160835.

11. Roser, A.-E., Caldi Gomes, L., Schünemann, J., Maass, F., and Lingor, P. (2018). Circulating miRNAs as Diagnostic Biomarkers for Parkinson's Disease. Front. Neurosci. *12*, 625. https://doi.org/10.3389/fnins.2018.00625.

12. Burgos, K., Malenica, I., Metpally, R., Courtright, A., Rakela, B., Beach, T., Shill, H., Adler, C., Sabbagh, M., Villa, S., et al. (2014). Profiles of Extracellular miRNA in Cerebrospinal Fluid and Serum from Patients with Alzheimer's and Parkinson's Diseases Correlate with Disease Status and Features of Pathology. PLoS One *9*, e94839. https://doi.org/10.1371/journal.pone.0106174.

13. Ćwiklińska, A., Procyk, G., Koziorowski, D., and Szlufik, S. (2024). The role of MicroRNAs in Progressive Supranuclear Palsy-A Systematic Review. Int. J. Mol. Sci. *25*, 8243. https://doi.org/10.3390/ijms25158243.

14. Pavelka, L., Rauschenberger, A., Hemedan, A., Ostaszewski, M., Glaab, E., and Krüger, R.; NCER-PD Consortium (2024). Converging peripheral blood microRNA profiles in Parkinson's disease and progressive supranuclear palsy. Brain Commun. *6*, fcae187. https://doi.org/10.1093/braincomms/fcae187.

15. Schulz, J., Takousis, P., Wohlers, I., Itua, I.O.G., Dobricic, V., Rücker, G., Binder, H., Middleton, L., Ioannidis, J.P.A., Perneczky, R., et al. (2019). Meta-analyses identify differentially expressed microRNAs in Parkinson's disease. Ann. Neurol. *85*, 835–851. https://doi.org/10.1002/ana.25490.

16. Todorov, H., Weiβbach, S., Schlichtholz, L., Mueller, H., Hartwich, D., Gerber, S., and Winter, J. (2024). Stage-specific expression patterns and co-targeting relationships among miRNAs in the developing mouse cerebral cortex. Commun. Biol. *7*, 1366. https://doi.org/10.1038/s42003-024-07092-7.

17. Margis, R., Margis, R., and Rieder, C.R.-M. (2011). Identification of blood microRNAs associated with Parkinson's disease. J. Biotechnol. *152*, 96–101. https://doi.org/10.1016/j.jbiotec.2011.01.023.

18. Vallelunga, A., Ragusa, M., Di Mauro, S., Iannitti, T., Pilleri, M., Biundo, R., Weis, L., Di Pietro, C., De Iuliis, A., Nicoletti, A., et al. (2014). Identification of circulating microRNAs for the differential diagnosis of Parkinson's disease and Multiple System Atrophy. Front. Cell. Neurosci. *8*, 156. https://doi.org/10.3389/fncel.2014.00156.

19. Qian, X., Song, H., and Ming, G.-L. (2019). Brain organoids: advances, applications and challenges. Development *146*, dev166074. https://doi.org/10.1242/dev.166074.

20. Louise Nickels, S., Modamio, J., Mendes-Pinheiro, B., Monzel, A.S., Betsou, F., and Schwamborn, J.C. (2020). Reproducible generation of human midbrain organoids for *in vitro* modeling of Parkinson's disease. Stem Cell Res. *46*, 10187. https://doi.org/10.1016/j.scr.2020.101870.

21. Parrotta, E.I., Lucchino, V., Zannino, C., Valente, D., Scalise, S., Bressan, D., Benedetto, G.L., Iazzetta, M.R., Talarico, M., Gagliardi, M., et al. (2025). Modeling Sporadic Progressive Supranuclear Palsy in 3D Midbrain Organoids: Recapitulating Disease Features for In Vitro Diagnosis and Drug Discovery. Ann. Neurol. *97*, 845–859. https://doi.org/10.1002/ana.27172.

22. Antón-Bolaños, N., Faravelli, I., Tyler, F., Andreadis, S., Kastli, R., Trattato, S., Adiconis, X., Wei, A., Kumar, A.S., Di Bella, D.J., et al. (2024). Brain Chimeroids reveal individual susceptibility to neurotoxic triggers. Nature *631*, 1–8. https://doi.org/10.1038/s41586-024-07578-8.

23. Benedetto, G., Zannino, C., Valente, D., Covello, R., Scalise, S., Lucchino, V., Quattrone, A., Parrotta, E.I., Quattrone, A., and Cuda, G. (2025). Generation of hiPSCs lines from three sporadic Parkinson's disease patients. Stem Cell Res. *82*, 103632. https://doi.org/10.1016/j.scr.2024.103632.

24. Harper, J.W., Ordureau, A., and Heo, J.-M. (2018). Building and decoding ubiquitin chains for mitophagy. Nat. Rev. Mol. Cell Biol. *19*, 93–108. https://doi.org/10.1038/nrm.2017.129.

25. Nag, S., Szederkenyi, K., Yip, C.M., and McQuibban, G.A. (2023). Protocol for evaluating mitochondrial morphology changes in response to CCCP-induced stress through oper-source image processing software. STAR Protoc. *4*, 102745. https://doi.org/10.1016/j.xpro.2023.102745.

26. Krauskopf, J., Verheijen, M., Kleinjans, J.C., de Kok, T.M., and Caiment, F. (2015). Development and Regulatory Application of Microrna Biomarkers. Biomark. Med. *9*, 1137–1151. https://doi.org/10.2217/bmm.15.50.

27. Meza-Sosa, K.F., Valle-García, D., Pedraza-Alva, G., and Pérez-Martínez, L. (2012). Role of microRNAs in central nervous system development and pathology. J. Neurosci. Res. *90*, 1–12. https://doi.org/10.1002/jnr.22701.

28. Sharma, S., and Lu, H.-C. (2018). microRNAs in Neurodegeneration: Current Findings and Potential Impacts. J. Alzheimers Dis. Parkinsonism *8*, 420. https://doi.org/10.4172/2161-0460.1000420.

29. Juźwik, C.A., S Drake, S., Zhang, Y., Paradis-Isler, N., Sylvester, A., Amar-Zifkin, A., Douglas, C., Morquette, B., Moore, C.S., and Fournier, A.E. (2019). microRNA dysregulation in neurodegenerative diseases: A systematic review. Prog. Neurobiol. *182*, 101664. https://doi.org/10.1016/j.pneurobio.2019.101664.

30. Jusop, A.S., Thanaskody, K., Tye, G.J., Dass, S.A., Wan Kamarul Zaman, W.S., and Nordin, F. (2023). Development of brain organoid technology derived from iPSC for the neurodegenerative disease modelling: a glance through. Front. Mol. Neurosci. *16*, 1173433. https://doi.org/10.3389/fnmol.2023.1173433.

31. Becerra-Calixto, A., Mukherjee, A., Ramirez, S., Sepulveda, S., Sinha, T., Al-Lahham, R., De Gregorio, N., Gherardelli, C., and Soto, C. (2023). Lewy Body-like Pathology and Loss of Dopaminergic Neurons in Midbrain Organoids Derived from Familial Parkinson's Disease Patient. Cells *12*, 625. https://doi.org/10.3390/cells12040625.

32. Gao, J., Wang, L., Liu, J., Xie, F., Su, B., and Wang, X. (2017). Abnormalities of Mitochondrial Dynamics in Neurodegenerative Diseases. Antioxidants *6*, 25. https://doi.org/10.3390/antiox6020025.

33. Wong, T.-S., Li, G., Li, S., Gao, W., Chen, G., Gan, S., Zhang, M., Li, H., Wu, S., and Du, Y. (2023). G protein-coupled receptors in neurodegenerative diseases and psychiatric disorders. Signal Transduct. Target. Ther. *8*, 177. https://doi.org/10.1038/s41392-023-01427-2.

34. Sushma, A.C.M., and Mondal, A.C. (2019). Role of GPCR signaling and calcium dysregulation in Alzheimer's disease. Mol. Cell. Neurosci. *101*, 103414. https://doi.org/10.1016/j.mcn.2019.103414.

35. Chen, Q., Deng, N., Lu, K., Liao, Q., Long, X., Gou, D., Bi, F., and Zhou, J. (2021). Elevated plasma miR-133b and miR-221-3p as biomarkers for early Parkinson's disease. Sci. Rep. *11*, 15268. https://doi.org/10.1038/s41598-021-94734-z.

36. Kim, J., Inoue, K., Ishii, J., Vanti, W.B., Voronov, S.V., Murchison, E., Hannon, G., and Abeliovich, A. (2007). A MicroRNA feedback circuit in midbrain dopamine neurons. Science *317*, 1220–1224. https://doi.org/10.1126/science.1140481.

37. Margis, R., Margis, R., and Carlos, R.M.R. (2011). Identification of blood microRNAs associated to Parkinson's disease. J. Biotechnol. *152*, 96–101. https://doi.org/10.1016/j.jbiotec.2011.01.023.

38. Nonaka, W., Takata, T., Iwama, H., Komatsubara, S., Kobara, H., Kamada, M., Deguchi, K., Touge, T., Miyamoto, O., Nakamura, T., et al. (2022). A cerebrospinal fluid microRNA analysis: Progressive supranuclear palsy. Mol. Med. Rep. *25*, 88. https://doi.org/10.3892/mmr.2022.12604.

39. Li, L., Ren, J., Pan, C., Li, Y., Xu, J., Dong, H., Chen, Y., and Liu, W. (2021). Serum miR-214 Serves as a Biomarker for Prodromal Parkinson's Disease (2021). Front. Aging Neurosci. *13*, 700959. https://doi.org/10.3389/fnagi.2021.700959.

40. Salaramoli, S., Hamid, R.J., and Hashemy, S.I. (2023). Salivary Biomarkers: Noninvasive Ways for Diagnosis of Parkinson's Disease. Neurol. Res. Int. *2023*, 3555418. https://doi.org/10.1155/2023/3555418.

41. Boscher, E., Goupil, C., Petry, S., Keraudren, R., Loiselle, A., Planel, E., and Hébert, S.S. (2021). MicroRNA-138 Overexpression Alters Aβ42 Levels and Behavior in Wildtype Mice (2021). Front. Neurosci. *14*, 591138. https://doi.org/10.3389/fnins.2020.591138.

42. Edgar, R., Domrachev, M., and Lash, A.E. (2002). Gene Expression Omnibus: NCBI gene expression and hybridization array data repository (2002). Nucleic Acids Res. *30*, 207–210. https://doi.org/10.1093/nar/30.1.207.

43. Parrotta, E.I., Scalise, S., Taverna, D., De Angelis, M.T., Sarro, G., Gaspari, M., Santamaria, G., and Cuda, G. (2019). Comprehensive proteogenomic analysis of human embryonic and induced pluripotent stem cells. J. Cell Mol. Med. *23*, 5440–5453. https://doi.org/10.1111/jcmm.14426.

44. Sozzi, E., Nilsson, F., Kajtez, J., Parmar, M., and Fiorenzano, A. (2022). Generation of Human Ventral Midbrain Organoids Derived from Pluripotent Stem Cells. Curr. Protoc. *2*, e555. https://doi.org/10.1002/cpz1.555.

45. Langmead, B., Trapnell, C., Pop, M., and Salzberg, S.L. (2009). Ultrafast and memory-efficient alignment of short DNA sequences to the human genome. Genome Biol. *10*, R25. https://doi.org/10.1186/gb-2009-10-3-r25.

46. Friedländer, M.R., Mackowiak, S.D., Li, N., Chen, W., and Rajewsky, N. (2012). miRDeep2 accurately identifies known and hundreds of novel microRNA genes in seven animal clades. Nucleic Acids Res. *40*, 37–52. https://doi.org/10.1093/nar/gkr688.

47. Wen, M., Shen, Y., Shi, S., and Tang, T. (2012). miREvo: An Integrative microRNA Evolutionary Analysis Platform for next-generation sequencing experiments. BMC Bioinf. *13*, 140. https://doi.org/10.1186/1471-2105-13-140.

48. Ru, Y., Kechris, K.J., Tabakoff, B., Hoffman, P., Radcliffe, R.A., Bowler, R., Mahaffey, S., Rossi, S., Calin, G.A., Bemis, L., and Theodorescu, D. (2014). The multiMiR R package and database: integration of microRNA-target interactions along with their disease and drug association. Nucleic Acids Res. *42*, e133. https://doi.org/10.1093/nar/gku631.

49. Cui, S., Yu, S., Huang, H.-Y., Lin, Y.-C.-D., Huang, Y., Zhang, B., Xiao, J., Zuo, H., Wang, J., Li, Z., et al. (2025). miRTarBase 2025: updates to the collection of experimentally validated microRNA-target interactions. Nucleic Acids Res. *53*, D147–D156. https://doi.org/10.1093/nar/gkae1072.

50. Wu, T., Hu, E., Xu, S., Chen, M., Guo, P., Dai, Z., Feng, T., Zhou, L., Tang, W., Zhan, L., et al. (2021). clusterProfiler 4.0: A universal enrichment tool for interpreting omics data. Innovation *2*, 100141. https://doi.org/10.1016/j.xinn.2021.100141.

STAR★METHODS

KEY RESOURCES TABLE

REAGENT or RESOURCE	SOURCE	IDENTIFIER
Antibodies		
p-α-synuclein (Ser129) (1:500)	Cell Signaling Technology	Cat#23706: RRID:AB_2798868
α-synuclein oligomeric (1:500)	Merck Millipore	Cat#ABN2265; RRID:AB_2910172
PGC-1α (1:100)	Santa Cruz Biotechnology	Cat#sc-518025; RRID:AB_2890187
NDUFS1 (1:5000)	Abcam	Cat#AB169540; RRID:AB_2687932
NRF2 (1:1000)	Cell Signaling Technology	Cat#12721; RRID:AB_2715528
PARKIN (1:500)	Santa Cruz Biotechnology	Cat#sc-32282; RRID:AB_628104
BAX (1:500)	Santa Cruz Biotechnology	Cat#sc-20067; RRID:AB_626726
BCL-XL (1:1000)	Cell Signaling Technology	Cat#2762; RRID:AB_10694844
GAPDH (1:1000)	Bioss, ThermoFisher Scientific	Cat#BS-10900R; RRID:AB_3661955
Peroxidase AffiniPure Donkey Anti-Rabbit IgG (1:10000)	Jackson ImmunoResearch	Cat#711-035-152; RRID:AB_10015282
NANOG (rabbit) (1:200)	Invitrogen, ThermoFisher Scientific	Cat#PA1-097; RRID:AB_2539867
OCT4 (1:200)	Cell Signaling Technology	Cat#75463; RRID:AB_2799870
SOX2 (1:500)	Abcam	Cat#Ab97959; RRID:AB_2341193
TRA1-60 (1:100)	Invitrogen, ThermoFisher Scientific	Cat#41-1000; RRID:AB_2533494
BRAT (1:20)	R&D System	Cat#AF2085; RRID:AB_2200235
NESTIN (1:1000)	STEMCELL Technologies	Cat#60091; RRID:AB_2650581
SOX17 (1:20)	R&D System	Cat#AF1924; RRID:AB_355060
FOXA2 (1:1000)	Santa Cruz Biotechnology	Cat#sc-101060; RRID:AB_1124660
LMX1A (1:200)	Invitrogen, ThermoFisher Scientific	Cat#PA5-115517; RRID:AB_2900153
ZO1 (1:300)	Invitrogen, ThermoFisher Scientific	Cat#33-9100; RRID:AB_87181
GIRK2 (1:100)	Abcam	Cat#Ab65096; RRID:AB_1139732
CALB (1:200)	Cell Signaling Technology	Cat#BK13176S; RRID: AB_2687400
TH (1:100)	Invitrogen, ThermoFisher Scientific	Cat#MA1-24654; RRID:AB_795666
DDC (1:200)	Invitrogen, ThermoFisher Scientific	Cat#PA547512; RRID:AB_2609231
NFL (1:100)	Cell Signaling Technology	Cat#2837; RRID: AB_823575
MAP2 (1:1000)	Invitrogen, ThermoFisher Scientific	Cat#PA-10005; RRID: AB_1076848
TH (1:2000)	Antibodies	Cat#A104316-100
TOM20 (1:400)	Proteintech	Cat#66777; RRID:AB_2919694
Anti-Rabbit IgG Alexa Fluor 488 PLUS (1:2000)	Life Technologies, ThermoFisher Scientific	Cat#A32731; RRID:AB_2633280
Anti-Rabbit IgG Alexa Fluor 594 (1:500)	Life Technologies, ThermoFisher Scientific	Cat#A-11012; RRID:AB_141359
Anti-Chicken IgY (H + L) Alexa Fluor 594 (1:200)	Life Technologies, ThermoFisher Scientific	Cat#A-32759; RRID:AB_2762829
Anti-Mouse IgG Alexa Fluor 488 (1:2000)	Life Technologies, ThermoFisher Scientific	Cat#A-11001; RRID:AB_2534069
Anti-Goat IgG Alexa Fluor 594 (1:500)	Life Technologies, ThermoFisher Scientific	Cat#A-11058; RRID:AB_142540
Anti-Mouse IgG Alexa Fluor 594 (1:200)	Life Technologies, ThermoFisher Scientific	Cat#A-11005; RRID:AB_141372
Deposited data		
GEO	Series accession number GSE294029	
Oligonucleotides		
OCT4	GGAGGAAGCTGACAACAATGAA	GGCCTGCACGAGGGTTT
NANOG	TGCAAGAACTCTCCAACATCCT	ATTGCTATTCTTCGGCCAGTT
SOX2	ATGCACCGCTACGACGTGA	CTTTTGCACCCCTCCCATTT
GATA4	GGCCTGTCATCTCACTACGG	ATGGCCAGACATCGCACT
HAND1	CCAGCTACATCGCCTACCTG	CCGGTGCGTCCTTTAATCCT
TUBB3	AACGAGGCCTCTTCTCACAA	TTTTCACACTCCTTCCGCAC

(*Continued on next page*)

Continued

REAGENT or RESOURCE	SOURCE	IDENTIFIER
CNPY1	GGAAGACCCTGTGACGAAGG	TCCTGGGCGATAAGTGAGGA
CORIN	CCCCGGGAAACTGCAATGTA	GCGATGCTCTGTTGTGGGAT
EN1	GCCCGTGGTCAAAACTGACT	GGAACTCCGCCTTGAGTCTC
NGN2	ACATGGACTATTGGCAGCCC	AGTGAGATGGTTTCCAGGGC
FOXA2	CTGGTCGTTTGTTGTGGCTG	CGTGTTCATGCCGTTCATCC
LMX1A	AACATGCTGGACGGCCTAAA	ATGCCAGAAGCTGTCGTTGA
LMX1B	CGGACTGCGCCAAGATGTT	TTGACTCGCATCAGGAAGCG
SHH	TGGACATCACCACGTCTGAC	GGAAGCAGCCTCCCGATTT
TH	TGTACTGGTTCACGGTGGAGT	TCTCAGGCTCCTCAGACAGG
OTX1	CGTTCACAGCTGGACGTG	CTTTCGGAGCCCGAGCTC
OTX2	CTGTTTGCCAAGACCCGGTA	TGGCCACTTGTTCCACTCTC
NURR1	TGCCGATTTCAGAAGTGCCT	CGAGGGCACTGATCAGACTC
DDC	GCCGCTATCATGGAGAAGCT	AGAAAGGAATCAGGCCAGCC
GIRK2	CACATCAGCCGAGATCGGAC	GGTAGCGATAGGTCTCCCTCA
CALB1	ATCCCTCATCACAGCCTCAC	TTTGCCCATACTGATCCACA
DAT	GTCTGTTTGGATTGACGCGG	AAGGAGAAGACGACGAAGCC
CCNB1	GTTGGTGTCACTGCC	TGGCCAAAGTATGTT
POLQ	GGTCTGATCAATCGC	AGCAGATACCCTCGG
SLC7A11	CTGACCATCTGGACGGTGTG	TGAGGAGTTCCACCCAGACT
QPCTL	CTCACCCTTGCCTGCCATTA	CGCCTCTTCACCATCCAAGA
REST	CTCATACAGGAGAACGCCCA	TGCATGGCGGGTTACTTCAT
RPL7L1	ATGATTCCTGGCGGCAGAAA	TTGCAATGGTTCTCTGCACC
VPS13A	GCTGGCTATGGTCTTGGTCA	GTTGGATCAACTGCTGTTTCACT
VIM	TGAAGGAGGAAATGGCTCGT	CCTCAGGTTCAGGGAGGAAA
SOX9	AGCTCTGGAGACTTCTGAACGAGA	CGTTCTTCACCGACTTCCTCCGC
CDK6	CCGTTTCGTGGCGTTGAAG	TCTGTTCGTGACACTGTGCA
GJA1	AGAACTCAAGGTTGCCCAAA	GATGATGTAGGTTCGCAGCA
ZNF215	AGGAACCTGAATTCATTGCGT	AGGCATCTGAAGAAGGGTGT
ZZZ3	ACCCTCAGAGGCAAGACTCA	CTGAGCCTCGAGTACAGCAA
SESN3	TGAAGAGGCGTCTCAAGAAGAA	CTCTTCTCCTCGTCTGGCAA
CXCR4	CTGGCCTTCATCAGTCTGGA	TCATCTGCCTCACTGACGTT
RB1CC1	CTTGAAGATCGGCTCTACGC	TCATCAACTGATTTGCGTGAC
HIF1A	GCCAGATCTCGGCGAAGTAA	ACCATAACAAAACCATCCAAGGC
ATF6	TGCTAGGGTTAGAGGCGAGA	CACAGACAACTCTTCGCTTTGG
GSK3B	CCACAGAACCTCTTGTTGGA	CGTGTAATCAGTGGCTCCAA
RPS8	GGCTATGTGCTAGAGGGCAA	CAGGCAACATAAATGTGGGAACA
RPS15A	CTTATTAGGCCGTGCTCCAA	TTCTGCCATTTTTCCAGGTC
BRCA1	TGGATTTATCTGCTCTTCGCGT	GGACACTGTGAAGGCCCTTT
USP1	AGAGGACTTGGGGAAGTGTGA	TTCACATTCCAAGCAACGCG
HNRNPU	CACTTCGATGACACAGTGGT	GTGACCAGCCAATACGAACT
CDK3	TCAAGGAACTGAAGCACCCC	TGAGTGGCAGAAACTCACCC
EN2	TGGGTCTACTGTACGCGCTA	CCGTCAGGTACCTGTTGGTC
ADAR	CAGACCCGCGGAGTTTCC	TGGTACCTGAGCTGTCTGTG
ZNF480	CCCTGGTCTGGTGAGAGTGA	CCCTTTCATCTGGAAATAGCTCCA
SPB1	CCCCAATGTGGTGACTCTCC	ACAAGCCAAACGTAGAGCCA
CANX	ATTGAGGACCCAGAAGACCG	CTGCGTCTGGATCAGGTACG
CCNE2	GGGGGATCAGTCCTTGCATT	TGTCATGAACATATCTGCTCTCCT
SOD2	CACTAGCAGCATGTTGAGCC	CCTGGTACTTCTCCTCGGTG
GPX1	TATCGAGAATGTGGCGTCCC	CCGGACGTACTTGAGGGAAT

(*Continued on next page*)

Continued

REAGENT or RESOURCE	SOURCE	IDENTIFIER
NRF2	CATCCAGTCAGAAACCAGTGG	AATGAAGACTGGGCTCTCGA
MFN2	TGCTAAGGAGGTGCTCAACG	CGTGTGCTGCTCAAACTTGG
FIS1	GAGCACGCAGTTTGAGTACG	ACCCGCGGACGTACTTTAAG
OPA1	TGCCTGACATTGTGTGGGAA	AGAGAAGTAGGTCAGAAGCTCCT
DRP1	ACCCGTGGATGATAAAAGTGCT	AGGTTCGCCCAAAAGTCTCA
MFN1	CCCTCTTGAGAGATGACCTGG	GGAAAGCCGCTCATTCACCT
BAX	GGACGAACTGGACAGTAACATGG	GCAAAGTAGAAAAGGGCGACAAC
FAS	GGAGTACACAGACAAAGCCCA	TTTGGTGCAAGGGTCACAGT
CELF2	GCCAGATAGAAGAATGCCGGA	GTGCCATTGCCCTTGTAGA
PEG3	GGGCCACTCATCAAGATCCA	TTCCCGATTTGGAACTGCGT
GAPDH	TCCTCTGACTTCAACAGCGA	GGGTCTTACTCCTTGGAGGC
Critical commercial assay		
Assay ID	475360	hsa-miR 5683
Assay ID	464290	hsa-miR 3085-3p
Assay ID	003188	hsa-miR 124-3p
Assay ID	462668	hsa-miR 219b-5p
Assay ID	002144	hsa-miR 138-2-3p
Assay ID	002356	hsa-miR 873-5p
Assay ID	002390	hsa-miR 219a-2-3p
Assay ID	000437	hsa-miR 100-5p
Assay ID	002222	hsa-miR 1-3p
Assay ID	002315	hsa-miR 10b-3p
Assay ID	001187	hsa-miR 140-5p
Assay ID	000200	cell-miR 39-3p
Assay ID	001973	snRNA U6
Software and algorithms		
GraphPadPrism (version 9.3.1)		N/A
ImageJ Fiji		N/A
Biorender		N/A

EXPERIMENTAL MODEL AND STUDY PARTICIPANT DETAILS

All experimental protocols were approved by the Institutional Review Board (IRB) of the "*Comitato Etico Territoriale Regione Calabria"* (**approval number #143, 13-05-2024**), in accordance with ethical guidelines and regulatory standards. Informed consent was obtained from all participants prior to sample collection. The study was conducted in compliance with the principles outlined in the Declaration of Helsinki. The use of human induced pluripotent stem cells (iPSCs) was approved by the Ethics Committee of the University of Catanzaro, with strict adherence to protocols ensuring donor anonymity and data protection.

METHOD DETAILS

Generation of PD patient-induced pluripotent stem cells (iPSCs)

The generation and characterization of healthy donor and PSP-RS patient-derived hiPSC lines were previously described,[21] with the exception of the HC_001-line, detailed previously.[43] For this study, we additionally recruited four sporadic PD patients, carefully matched by sex and age to existing iPSC donors (Ethnicity of all lines: Caucasian). Blood samples were collected in accordance with protocols approved by the University 'Magna Graecia' of Catanzaro and the Azienda Ospedaliero-Universitaria "Renato Dulbecco" of Catanzaro, Italy. PD iPSC lines were generated from peripheral blood mononuclear cells (PBMCs) using the CytoTune^{TM}-iPS 2.0 Sendai Reprogramming Kit (Thermo Fisher Scientific), following the manufacturer's instructions with minor modifications. A detailed protocol is available in.[21] The characterization of iPSC lines PD-1, PD-2, and PD-4 has been reported previously.[23] In this study, we further characterized the PD-3 iPSC line, confirming its expression of pluripotency markers and trilineage differentiation capacity, validating its use for downstream disease modeling (Figure S1).

Generation of midbrain organoids (MOs)

Midbrain organoids (MOs) were generated based on a previously established protocol,[44] with modifications in the initial phase to enable the formation of multi-donor organoids by pooling healthy and patient-derived iPSCs, as described in.[21] iPSCs were cultured on Matrigel-coated dishes (Corning, Corning, NY, USA) in mTeSR1 medium (StemCell Technologies, Vancouver, BC, Canada) and dissociated using Gibco™ StemPro™ Accutase™ (Thermo Fisher Scientific, Waltham, MA, USA). Cell suspensions from three healthy controls, four PSP-RS patients, and four PD patients were mixed in equal ratios. A total of 10,000 cells per well were seeded in ultra-low attachment 96-well U-bottom plates (Corning, NY, USA) in mTeSR1 medium with 10 μM Y-27632 (Miltenyi Biotec, Bergisch-Gladbach, Germany) to initiate MO formation. After three days, embryoid bodies (EBs) were transferred to a differentiation medium consisting of a 1:1 mix of DMEM/F12 and Neurobasal medium, supplemented with 1:100 N2, 200 mM L-glutamine, and 10,000 U/mL penicillin/streptomycin (Thermo Fisher Scientific). The medium was further enriched with 10 μM SB431542, 100 ng/mL recombinant human Noggin (rhNoggin), 300 ng/mL SHH-C24II, and 1.5 μM CHIR99021 (Miltenyi Biotec). On day 8, the medium was supplemented exclusively with 100 ng/mL FGF-8b (Miltenyi Biotec). From days 11–14, organoids were maintained in Neurobasal medium with 1:50 B27 without vitamin A, 200 mM L-glutamine, and antibiotics, along with 100 ng/mL FGF-8b, 20 ng/mL brain-derived neurotrophic factor (BDNF), and 200 μM L-ascorbic acid. On day 14, organoids were embedded in Matrigel Matrix (Corning) and transferred to long-term differentiation medium containing B27 supplement, 20 ng/mL BDNF, 10 ng/mL glial cell line-derived neurotrophic factor (GDNF) (R&D Systems, Bio-Techne), 200 μM L-ascorbic acid, 500 μM cyclic AMP (Sigma-Aldrich, St. Louis, MO, USA), and 1 μM DAPT (Tocris, Bio-Techne). This multi-donor MO approach enhances the modeling of inter-individual variability, offering a more representative platform for investigating neurodegenerative disease mechanisms.

RNA extraction, reverse transcription, and quantitative real-time PCR

Total RNA was extracted using TRIzol Reagent (Thermo Fisher Scientific), following the manufacturer's instructions. Reverse transcription was performed using the High-Capacity cDNA Reverse Transcription Kit (Thermo Fisher Scientific). Quantitative real-time PCR (qPCR) was carried out using the SensiFAST SYBR Hi-ROX Kit (Meridian Bioscience) on a QuantStudio™ 7 Pro Real-Time PCR System (Applied Biosystems). Gene expression levels were analyzed using the comparative Ct (cycle threshold) method, with glyceraldehyde 3-phosphate dehydrogenase (GAPDH) used as the endogenous control for normalization. For miRNA validation in individual organoids, reverse transcription was performed using the TaqMan™ MicroRNA Reverse Transcription Kit (Thermo Fisher Scientific), followed by quantitative PCR using the TaqMan™ Fast Advanced Master Mix on a StepOnePlus™ Real-Time PCR System (Applied Biosystems). Primer sequences and TaqMan MicroRNA Assay used in this study are listed in the key resources table in the STAR Methods section.

Immunofluorescence

For immunofluorescence analysis, organoids were fixed in 4% paraformaldehyde (PFA) at room temperature. After fixation, they were incubated overnight in a 30% (w/v) sucrose solution at 4°C on an orbital shaker for cryoprotection, then embedded in Optimal Cutting Temperature (OCT) compound (Avantor). Organoids were sectioned at 20 μm thickness and post-fixed in 4% PFA for 10 min. Sections were then blocked for 1 h at room temperature in a solution containing 5% (v/v) goat serum (Thermo Fisher Scientific) and 0.3% (v/v) Triton X-100 (Sigma-Aldrich) in 1× PBS. Following blocking, sections were incubated overnight at 4°C with primary antibodies targeting specific proteins of interest. After primary incubation, sections were treated with Alexa Fluor 488-, 594-, or 647-conjugated secondary antibodies (Thermo Fisher Scientific) for 1 h at room temperature. Nuclear staining was performed using DAPI (Thermo Fisher Scientific), and coverslips were mounted with Fluormount Aqueous Mounting Medium (Sigma-Aldrich). Images were acquired using a MIKA Leica fluorescence microscopy system. A complete list of antibodies used is provided in the key resources table in the STAR Methods section.

Protein extraction and immunoblotting

Proteins were extracted from organoids by mechanical disruption through pipetting in RIPA buffer, composed of 150 mM sodium chloride, 1% Triton X-100, 0.5% sodium deoxycholate, 0.1% sodium dodecyl sulfate (SDS) (all from Sigma-Aldrich), and 50 mM Tris-HCl (pH 7.5; Gibco), supplemented with Halt™ Protease and Phosphatase Inhibitor Cocktail (Thermo Fisher Scientific). Extracts were sonicated using a Diagenode Bioruptor (10 cycles of 30 s ON/30 s OFF) and then incubated on ice for 30 min. Supernatants were collected by centrifugation at 21,000 × g for 1 h at 4°C to remove insoluble debris. Protein concentrations were determined using the Bradford assay (Bio-Rad). Equal amounts of protein (25 μg) were diluted in 1× Bolt™ LDS Sample Buffer with Bolt™ Reducing Agent (Thermo Fisher Scientific) and denatured at 70°C for 10 min. Proteins were resolved using either Bolt™ 4–12% Bis-Tris Plus gels with Bolt™ MES SDS running buffer (20×) or NuPAGE™ 3–8% Tris-Acetate gels with NuPAGE™ Tris-Acetate SDS buffer (20×), specifically for detecting oligomeric α-synuclein (Thermo Fisher Scientific). Proteins were transferred onto nitrocellulose membranes (Bio-Rad) using the Trans-Blot Turbo™ Transfer System (Bio-Rad). Membranes were blocked for 1 h at room temperature in 5% non-fat dry milk (PanReac AppliChem) to prevent non-specific binding. Primary antibodies were incubated overnight at 4°C, followed by 1 h incubation at room temperature with HRP-conjugated secondary antibodies (Jackson ImmunoResearch). Signals were detected using Clarity™ ECL substrate (Bio-Rad), and images were acquired with the Alliance™ Q9-Atom imaging system (Uvitec). Band intensities were quantified using ImageJ software, with GAPDH used as the internal loading control. The specific antibodies used for immunoblotting are listed the key resources table in the STAR Methods section.

QUANTIFICATION AND STATISTICAL ANALYSIS

Statistical analyses were performed using unpaired *t*-tests with Welch's correction or one-way ANOVA test with Tukey's correction in GraphPad Prism (version 9.3.1). Data are presented as the mean ± standard error of the mean (SEM), based on two or three biological replicates. Statistical significance is indicated as follows: $*p < 0.05$, $**p < 0.01$, $***p < 0.001$, and $****p < 0.0001$. All experiments—including Western blotting, immunofluorescence, and RT-qPCR—were conducted with technical replicates using at least three organoids from three independent differentiation batches.

miRNA sequencing

Library construction, quality control, and sequencing

Total RNA was used as the input material for small RNA library preparation. Adapters were first ligated to the 3′ and 5′ ends of the small RNA molecules. Following adapter ligation, first-strand complementary DNA (cDNA) synthesis was performed via reverse transcription primer hybridization. The resulting cDNA was then PCR-amplified to generate double-stranded cDNA libraries. Libraries were purified and size-selected to enrich for fragments with insert sizes between 18 and 40 base pairs. Final libraries were prepared for single-end sequencing (SE50) on an Illumina platform, with a read length of 50 bases. Library quality and concentration were assessed using a Qubit fluorometer (Thermo Fisher Scientific) and real-time PCR. Fragment size distribution was verified using a Bioanalyzer (Agilent Technologies). Qualified libraries were pooled based on effective concentration and desired sequencing depth, then sequenced on Illumina platforms for downstream analysis.

Bioinformatics analysis

Data preprocessing and quality control

Raw sequencing data in FASTQ format were processed using custom Perl and Python scripts. Clean reads were obtained by filtering out sequences containing poly-Ns, 5′ adapter contaminants, incomplete 3′ adapters or insert tags, as well as low-quality reads. Reads consisting of homopolymeric stretches (poly A, T, G, or C) were also excluded. Quality metrics, including Q20 and Q30 scores and GC content, were calculated to assess the overall data quality.

Mapping and miRNA identification

Cleaned small RNA tags were aligned to the reference genome using Bowtie,[45] allowing for zero or one mismatch. Known microRNAs (miRNAs) were identified using miRBase v22.0 as a reference. To detect novel miRNAs and examine the secondary structure of unannotated tags, we employed modified versions of *mirDeep2*[46] and *srna-tools-cli*. Custom scripts were used to quantify miRNA read counts and assess nucleotide bias at both the first base and across all positions of identified miRNAs. To eliminate non-miRNA tags, reads were also mapped to databases such as RepeatMasker and Rfam, and against species-specific genome annotations, filtering out tags derived from protein-coding genes, repeat elements, rRNAs, tRNAs, snRNAs, and snoRNAs.

Novel miRNA prediction

Novel miRNAs were predicted based on the characteristic hairpin structures of miRNA precursors. Software tools including *miREvo*[47] and *mirDeep2* were used to evaluate secondary structures, Dicer cleavage sites, and the minimum free energy of novel miRNA candidates. Additional custom scripts facilitated miRNA count generation and base bias analysis.

Annotation summary

All alignments and annotations were integrated and summarized. Because some small RNA tags could map to multiple categories, a hierarchical priority rule was applied: known miRNA > rRNA > tRNA > snRNA > snoRNA > repeat > gene > NAT-siRNA > novel miRNA > ta-siRNA. The proportion of rRNA was used as a sample quality metric, with values below 40% considered acceptable.

miRNA quantification and differential expression analysis

miRNA expression levels were quantified as transcripts per million (TPM) using the following formula: Normalized expression = (mapped read count/total reads) × 1,000,000 Differential expression analysis between experimental groups was performed using *DESeq2*. *p*-values were adjusted using the Benjamini–Hochberg method, with an adjusted p-value <0.05 considered statistically significant.

Target prediction and enrichment analysis

Target genes for differentially expressed miRNAs were predicted using the get_multimir function from the *multiMiR* R package,[48] focusing on experimentally validated targets in *miRTarBase*.[49]

Venn diagram analysis

To identify disease-associated miRNAs consistently upregulated across all three time points, Venn diagram analysis was performed using *Venny* (https://bioinfogp.cnb.csic.es/tools/venny/).

GO enrichment analysis

Gene Ontology (GO) enrichment analysis was performed on predicted target genes of differentially expressed miRNAs using the *ClusterProfiler* R package (v4.12.2[50]), considering all three GO domains: biological process, cellular component, and molecular function. Initially, we conducted enrichment analysis on the combined set of target genes from all selected miRNAs across the three comparison groups (PD vs. HC, PSP-RS vs. HC, and PSP-RS vs. PD). Subsequently, GO enrichment was performed for each selected miRNA individually, based on its predicted target genes, to uncover functional categories specifically associated with individual miRNA signatures.